BIOMEDICAL RESEARCH INSTITUTE (BRI)

FOUNDATION FOR RESEARCH AND TECHNOLOGY HELLAS (FORTH)

UNIVERSITY OF IOANNINA

FACULTY OF MEDICINE

Master's Thesis:

Mechanoresponsiveness of Lung Cancer Cells

Inter-institutional Interdepartmental Program of Postgraduate Studies
"Molecular – Cellular Biology and Biotechnology"

Supervisor: Prof. Evangelos Kolettas

Co-supervisor: Dr. Maria Georgiadou

Anastasia Androutsopoulou

Ioannina, 2024

Acknowledgements

This thesis was conducted at the Biomedical Research Institute (BRI) – Foundation for Research and Technology Hellas (FORTH), in collaboration with the Department of Medicine at the University of Ioannina.

I am profoundly grateful to my supervisor, Professor Evangelos Kolettas, and my co-supervisor, Research Scientist ‘C’ Maria Georgiadou, for providing me with the opportunity to undertake this research and for their invaluable guidance throughout the process.

A special thank you goes to Dr. Eugenia Roupakia, who played a pivotal role in the completion of this thesis. I am deeply grateful for her patience, and valuable advice.

I would also like to thank the other members of the lab for their collaborative spirit and for fostering a positive working environment. A heartfelt thank you to Margarita Maroudi, whose companionship on this journey brought joy to my days. I sincerely wish her every success in her future career.

Lastly, my deepest gratitude goes to the unsung heroes of this thesis—my parents, Tasos and Georgia. Their love, unwavering support and encouragement have been invaluable to me.

Table of Contents

Abstract

Lung cancer ranks as the leading cause of cancer mortality worldwide, primarily because it is often diagnosed at an advanced stage. Early symptoms are typically mild or mistaken for common respiratory issues, leading to delayed diagnosis. As a result, the disease frequently progresses to metastasis, significantly limiting treatment options.

Directed cell migration, a critical aspect of cancer metastasis, involves cells sensing and responding to signals from the extracellular matrix (ECM) or neighbouring cells, polarizing, and moving in a specified direction. While research has traditionally focused on soluble chemical factors influencing migration (chemotaxis), ECM stiffness has recently emerged as a significant mechanical cue affecting cell behaviour and migration. Increasing evidence suggests that increased ECM stiffness contributes to a pro-invasive tumour microenvironment, facilitating cancer progression.

Durotaxis, the directional migration towards regions of increasing stiffness, has been extensively studied in normal cells, but its role in cancer cell migration remains less understood. Solid tumours, including lung cancer, typically exhibit higher stiffness levels than normal tissues. Investigating the impact of increased ECM stiffness on lung cancer cell migration can provide new insights into the mechanisms driving metastasis and identify potential therapeutic targets to inhibit cancer progression.

In the framework of this Master's thesis, we evaluated the durotactic potential of four EGFR-driven Non-Small Cell Lung Cancer (NSCLC) cell lines using polyacrylamide (PA)-based hydrogels with a stiffness gradient of 0.5-22 kPa, mimicking the stiffness levels encountered by cells in healthy and cancerous lungs. Our experiments revealed a diverse range of migration modes in response to changes in extracellular stiffness. The HCC-827 and HCC-4006 cell lines exhibited the strongest durotactic migratory response on the softest regions of stiffness gradients (0.5–4 kPa), with decreased responsiveness on stiffer regions. The NCI-H2279 cell line demonstrated adurotactic behaviour, while the PC-9 cell line showed high heterogeneity, employing both durotaxis and negative durotaxis depending on the stiffness range of the gradient.

Furthermore, migration speed and distance increased at higher stiffness levels for primary tumour cell lines, while metastatic cells maintained constant values across the stiffness gradient. Finally, we found that actin cytoskeleton morphology (cell area and circularity) varied greatly across the stiffness gradient, offering no clear insights into the role of the actin cytoskeleton in cancer cell durotaxis.

This study underscores the importance of ECM stiffness in lung cancer cell migration and highlights the need for further research to fully understand the mechanistic underpinnings of durotaxis in cancer cells.

Περίληψη

Ο καρκίνος του πνεύμονα κατατάσσεται πλέον ως η κύρια αιτία θανάτου από καρκίνο παγκοσμίως, καθώς συχνά διαγιγνώσκεται σε προχωρημένο στάδιο. Τα πρώιμα συμπτώματα είναι τυπικά ήπια ή συγχέονται με κοινά αναπνευστικά προβλήματα, οδηγώντας σε μη έγκαιρη διάγνωση. Ως αποτέλεσμα, η ασθένεια συχνά προχωρά σε μετάσταση, περιορίζοντας σημαντικά τις θεραπευτικές επιλογές.

Η κυτταρική μετανάστευση, η οποία αποτελεί κρίσιμο στάδιο για τη μετάσταση του καρκίνου, περιλαμβάνει την ανίχνευση σημάτων από την εξωκυττάρια θεμέλια ουσία (ΕΘΟ) ή τα γειτονικά κύτταρα, την πόλωση των κυττάρων και τη μετακίνησή τους προς μια συγκεκριμένη κατεύθυνση. Ενώ η έρευνα παραδοσιακά επικεντρωνόταν σε διαλυτούς χημικούς παράγοντες που επηρεάζουν τη μετανάστευση (χημειοτακτισμός/chemotaxis), η ακαμψία (stiffness) έχει πρόσφατα αναδειχθεί ως ένα σημαντικό βιοφυσικό χαρακτηριστικό της ΕΘΟ που επηρεάζει τη συμπεριφορά και τη μετανάστευση των κυττάρων. Αυξανόμενα στοιχεία υποδεικνύουν ότι η αυξημένη ακαμψία της ΕΘΟ συμβάλλει στη δημιουργία ευνοϊκού μικροπεριβάλλοντος για την εξέλιξη του καρκίνου.

Η μετανάστευση προς περιοχές με αυξημένη ακαμψία (durotaxis) έχει μελετηθεί εκτενώς σε φυσιολογικά κύτταρα. Ωστόσο, ο ρόλος της στη μετανάστευση καρκινικών κυττάρων παραμένει άγνωστος. Οι συμπαγείς όγκοι, συμπεριλαμβανομένου του καρκίνου του πνεύμονα, παρουσιάζουν συνήθως υψηλότερα επίπεδα ακαμψίας από τους φυσιολογικούς ιστούς. Η διερεύνηση της επίδρασης της αυξημένης ακαμψίας της ΕΘΟ στη μετανάστευση των καρκινικών κυττάρων του πνεύμονα μπορεί να προσφέρει νέες γνώσεις για τους μηχανισμούς που οδηγούν στη μετάσταση και να εντοπίσει πιθανούς θεραπευτικούς στόχους για την αναστολή της εξέλιξης του καρκίνου.

Στα πλαίσια αυτής της μεταπτυχιακής διατριβής, αξιολογήσαμε το δυναμικό μετανάστευσης προς περιοχές με αυξημένη ακαμψία τεσσάρων κυτταρικών σειρών Μη Μικροκυτταρικού Καρκίνου του Πνεύμονα (ΜΜΚΠ) με μεταλλάξεις στο γονίδιο του Υποδοχέα Επιδερμικού Αυξητικού Παράγοντα (Epidermal Growth Factor Receptor, EGFR). Χρησιμοποιήθηκαν υδρογέλες πολυακρυλαμιδίου με διαβάθμιση ακαμψίας 0,5-22 kPa, η οποία μιμείται τα επίπεδα ακαμψίας που αντιλαμβάνονται τα κύτταρα στον υγιή και κακοήθη πνεύμονα. Τα πειράματά μας αποκάλυψαν μια ποικιλία τύπων μετανάστευσης σε απόκριση σε αλλαγές στην ακαμψία της ΕΘΟ. Οι κυτταρικές σειρές HCC-827 και HCC-4006 μετακινήθηκαν προς περιοχές αυξημένης ακαμψίας, με υψηλότερη απόδοση σε περιοχές χαμηλής διαβάθμισης ακαμψίας (0,5-4 kPa) και μειωμένη απόκριση σε περιοχές υψηλότερης ακαμψίας. Η κυτταρική σειρά NCI-H2279 δεν παρουσίασε καμία προτίμηση προς το επίπεδο ακαμψία, κάνοντας τυχαία μετανάστευση, ενώ η κυτταρική σειρά PC-9 παρουσίασε υψηλή ετερογένεια, υιοθετώντας διαφορετικό τύπο μετανάστευσης, ανάλογα με τη περιοχή που βρισκόταν στη διαβάθμιση ακαμψίας.

Επιπλέον, η ταχύτητα και η απόσταση που διανύθηκε κατά τη μετανάστευση αυξήθηκαν σε υψηλότερα επίπεδα ακαμψίας μόνο για τις κυτταρικές σειρές πρωτοπαθών όγκων, ενώ τα κύτταρα που προέρχονταν από μετάσταση διατήρησαν σταθερές τιμές σε όλα τα επίπεδα ακαμψίας. Τέλος, διαπιστώσαμε ότι η μορφολογία του κυτταροσκελετού ακτίνης ήταν πολύ ετερογενής σε όλο το εύρος της υδρογέλης, με αποτέλεσμα να μην

προσφέρει σαφείς ενδείξεις για τον ρόλο του κυτταροσκελετού ακτίνης στο φαινόμενο durotaxis των καρκινικών κυττάρων.

Αυτή η μελέτη υπογραμμίζει τη σημασία της ακαμψίας της ΕΘΟ στη μετανάστευση των καρκινικών κυττάρων του πνεύμονα και τονίζει την ανάγκη για περαιτέρω έρευνα ώστε να κατανοηθούν πλήρως οι μηχανιστικές βάσεις του φαινομένου durotaxis στα καρκινικά κύτταρα.

1. Introduction

1.1. Lung Cancer

1.1.1. Epidemiology of Lung Cancer

Lung cancer refers to malignant tumours that arise from the lung parenchyma or within the bronchi (Siddiqui, Vaqar, & Siddiqui, 2023). Smoking is the most important risk factor for the development of lung cancer; accounting for 80-90% of lung cancer cases worldwide (Corrales et al., 2020). Despite breakthroughs in treatment regimens, lung cancer remains one of the most frequent malignancies, representing approximately 12.4% of all cancer diagnoses (Siegel, Miller, & Jemal, 2020). According to the 2022 World Health Organization (WHO) classification, lung cancer is the second most prevalent cancer worldwide after breast cancer (***Figure 1***). Even though the number of patients afflicted with breast cancer is the highest, lung cancer is the leading cause of cancer mortality among both sexes, accounting for an estimated 2.2 million diagnoses and 1.8 million deaths – a figure that is constantly rising. The reason for this rise is that early symptoms may be mild or misdiagnosed as typical respiratory problems, resulting in a delayed diagnosis (Bradley, Kennedy, & Neal, 2019).

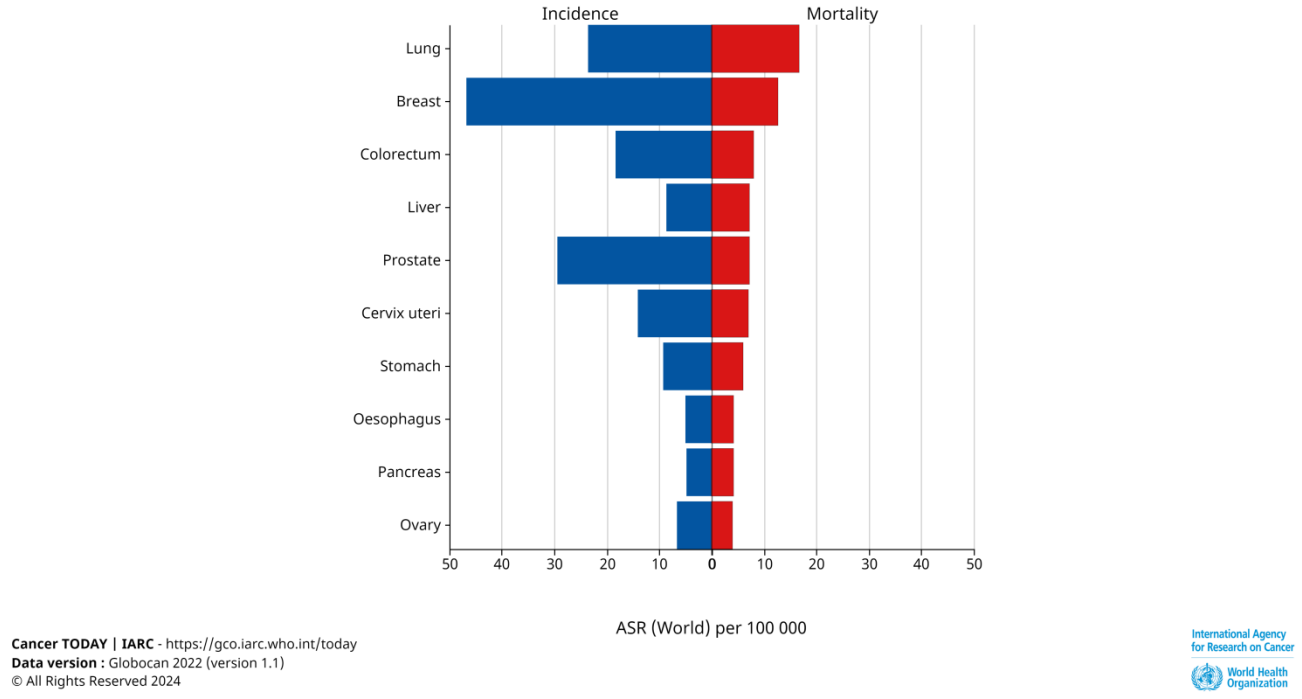

Figure 1. *Estimated age-standardized incidence and mortality rates in 2022, World, both sexes, all ages (Global Cancer Observatory, WHO).*

1.1.2. Types of Lung Cancer

As stated by the 2004 WHO lung cancer classification system (Travis, Brambilla, Muller-Hermelink, & Harris), lung cancer is mainly divided into two histological types: Small Cell Lung Cancer (SCLC), which accounts for roughly 15% of all lung cancer incidents, and Non-Small Cell Lung Cancer (NSCLC), which is responsible for approximately 85% of all lung cancer cases (***Figure 2***). NSCLC is characterized by larger cells and typically grows more slowly than SCLC. NSCLC is further classified into three subtypes: adenocarcinoma (LUAD), squamous-cell carcinoma (LUSC) and large-cell carcinoma (LCC) (Z. Chen, Fillmore, Hammerman, Kim, & Wong, 2014). LUAD is the most frequent subtype, accounting for over 40% of lung cancer cases and 15% of a 5-year survival rate due to late diagnosis and drug resistance (Shi et al., 2016). The standard approach for the identification of these four main types of lung cancer relies primarily on immunohistochemistry assays and then molecular analysis of the tumour. Over the last two decades, the introduction of molecular techniques to pathologic diagnosis has led to more accurate categorization of lung cancers (Meyerson, Franklin, & Kelley, 2004). Genome-wide association studies (GWAS) have been critical in finding novel molecular markers in lung cancer revealing a further sub-classification into the main types of lung malignancies, listed in the 2021 WHO Classification of Thoracic Tumours (Nicholson et al., 2022).

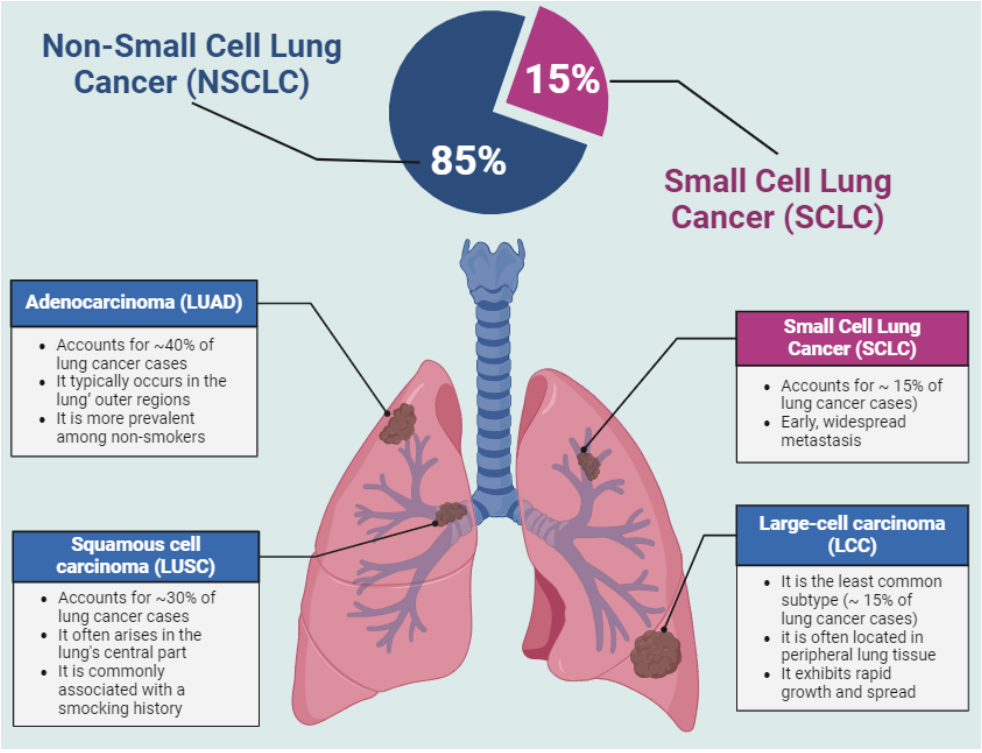

Figure 2. *Types of Lung Cancer (created using Biorender.com).*

1.1.3. Diagnosis and Treatment of Lung Cancer

Early detection of lung cancer is crucial. At early stages, surgery involving removal of either a portion of the lung or the entire lung is the main option for localized lung cancer treatment (Harðardottir et al., 2022).

However, lung cancer is frequently detected at an advanced stage, when treatment choices are limited. Specifically, almost half of lung cancer cases are diagnosed at advanced stage, when five-year survival rate is only 6% (Siegel, Miller, Fuchs, & Jemal, 2022). Early diagnosis is challenging, since early-stage lung cancer is asymptomatic (Birring & Peake, 2005). As the tumour develops, symptoms including cough, chest pain, and weight loss may be mistaken for other diseases, leading to differential diagnosis (Hyde & Hyde, 1974). When the disease has spread to distant organs, radiation therapy is given alone or in combination with chemotherapy or targeted drug therapy, when a specific malignant mutation has been identified. Namely, in cases of EGFR mutations, EGFR inhibitors, such as osimertinib or erlotinib, are used (García-Fernández, Fornaguera, & Borrós, 2020). However, the biggest disadvantage of these therapeutic approaches is the development of resistance mechanisms, leading to disease relapse (Ashrafi et al., 2022).

1.2. Introduction to Mechanobiology

Cells rely on signals from their surrounding environment in order to develop and function properly. These signals emanate from neighbouring cells and the extracellular matrix (ECM). Mechanobiology, an emerging and exciting field, investigates the mechanisms by which mechanical cues of the ECM shape cell behaviour (J. D. Humphrey, E. R. Dufresne, & M. A. Schwartz, 2014). Cells sense the mechanical properties of their environment, such as the stiffness of the extracellular matrix, through specific mechanosensors, and convert these mechanical stimuli into biochemical signals. This process, also called mechanotransduction, prompts a cascade of cellular responses, including proliferation, differentiation, polarization and migration.

1.2.1. The Extracellular Matrix at a Glance

The ECM is a multifaceted and dynamic three-dimensional network of macromolecules that surrounds cells providing mechanical support and influencing cellular behaviour through a variety of biochemical and biophysical signals. It is a complex mixture of water, proteins, and polysaccharides, primarily secreted and remodelled by fibroblasts (Alberts, 2017). While the fundamental organization remains consistent, there are two types of ECM; the interstitial matrix, which creates a three-dimensional porous network enveloping cells, and the pericellular or basement membrane, which is a thin sheet-like ECM located at tissue borders offering compartmentalization (Tsutsui et al., 2021).

Serving as a scaffold which allows cells to adhere, the ECM maintains tissue integrity and architecture, defining the characteristic shape and dimensions of organs and complex tissues. Through bioinformatics analysis of the human genome conducted as part of the Matrisome Project by Dr. Alexandra Naba and colleagues, approximately 1027 genes have been identified as responsible for expressing fundamental components of the human ECM (A. Naba et al., 2012). Some of the main components include collagens, proteoglycans (PGs), glycosaminoglycans (GAGs), elastin, elastic fibers, laminins and fibronectin, among other proteins (Kular, Basu, & Sharma, 2014). This protein diversity, as well as the widening variety of ECM

receptors found on cell surfaces, correlates with the evolution and development of complex functionally discrete tissues and organs in higher organisms (Hynes, 2009). Thus, different organs and tissues exhibit differential expression of ECM components.

In addition to serving as a structural component of tissues, the ECM plays crucial functional roles in influencing various cellular processes. ECM components, like collagen and fibronectin, through their engagement with cell surface receptors like integrins, mediate cell shape and migration (R. O. Hynes, 2002; Parisi et al., 2020). It also forms a dynamic tissue-specific "niche" that affects the stemness and differentiation of progenitor/stem cell populations (Gattazzo, Urciuolo, & Bonaldo, 2014; Walma & Yamada, 2020), as well as the proper function, properties and morphology of the differentiated cell types in that particular tissue, maintaining organ homeostasis in adulthood (T. R. Cox & Erler, 2011).

Each tissue has markedly distinct biomechanical properties, thus requires specific ECM phenotypes in order to function properly (Barros, Franco, & Müller, 2011; Csapo, Gumpenberger, & Wessner, 2020; McKee, Perlman, Morris, & Komarova, 2019). Nevertheless, the ECM phenotype can constantly be adapted according to biochemical or mechanical signals (T. R. Cox & Erler, 2011). This is a tightly controlled dynamic ECM remodelling procedure, during which the composition and concentration of matrix components could be altered and post-translational modifications, such as glycosylation, transglutamination and cross-linking, may occur (Erler & Weaver, 2009). Excessive or uncontrolled remodelling may lead or contribute in various serious pathological conditions including fibrosis and cancer (Girigoswami, Saini, & Girigoswami, 2021).

1.2.2. The Stiffness of the Extracellular Matrix

Matrix stiffness is defined as the extent to which the extracellular matrix resists deformation in response to an applied force. It is quantified in kilo Pascal (kPa), where one Pascal equals one Newton of force applied over one square meter (m^2). Tissue stiffness is measured by the Young's modulus, also known as elastic modulus, with the use of Atomic Force Microscopy (AFM). AFM is a specific type of microscopy, which uses a mechanical probe to contact with the sample surface, in order to measure its stiffness. Due to the small size of the probe tip, AFM can "sense" stiffness on the same scale (micron length) as cells can feel their matrices. However, this equipment is not accessible to every laboratory.

Each organ in the human body manifests a distinctive range of stiffness values (***Figure***), crucial for the optimal functionality of its constituent cells, under physiological conditions (D. E. Discher, P. Janmey, & Y.-l. Wang, 2005). However, pathological states, including fibrosis and cancer, can disrupt this balance, leading to altered organ stiffness. Notably, in cancer, tumour tissues generally exhibit higher stiffness compared to healthy tissues; for instance, the stiffness of solid lung cancers (20–30 kPa) markedly exceeds that of normal lung parenchyma (0.5–5 kPa) (Miyazawa et al., 2018). This shift in stiffness has emerged as a critical determinant in regulating tumour progression and metastasis (Emon, Bauer, Jain, Jung, & Saif, 2018; Jiang et al., 2022; Wei & Yang, 2016; Winkler, Abisoye-Ogunniyan, Metcalf, & Werb, 2020). Yet, an increase in ECM stiffness has been documented during embryonic development as well (K. A. Moore et al., 2005; Wang, Ji,

Wang, & Liu, 2023). Hence, gaining insight into the dynamic alterations in ECM stiffness during both physiological and pathological processes is imperative for comprehending its profound impact on cellular behaviour.

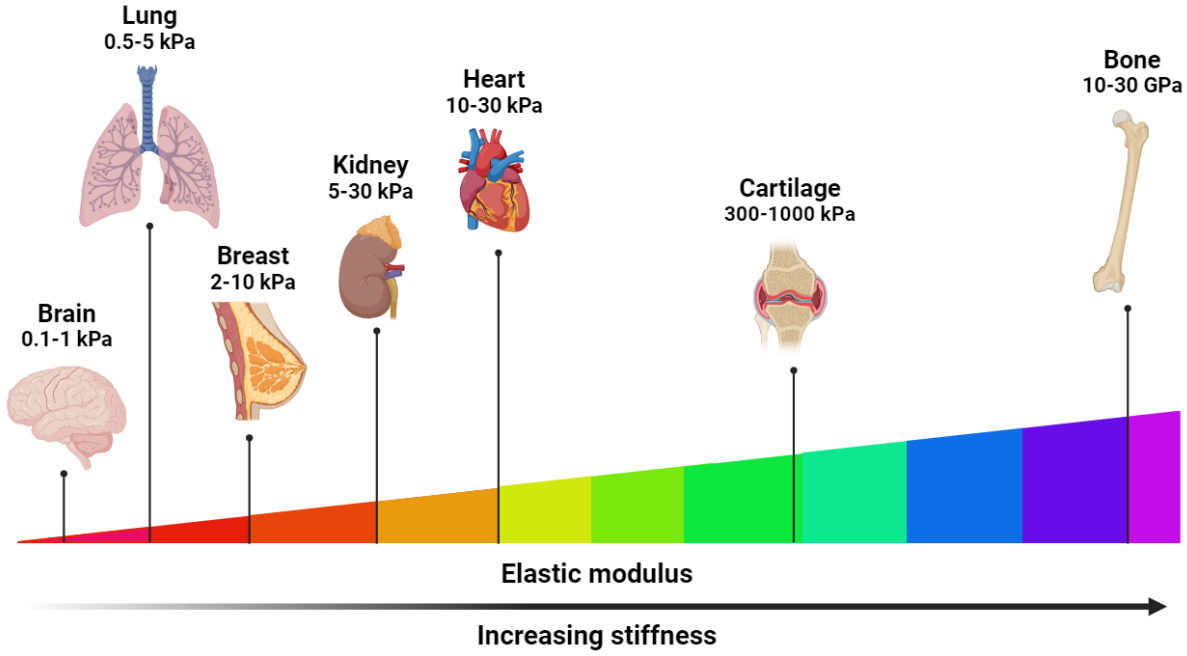

Figure 3. *Tissue stiffness in vivo (created using Biorender.com).*

1.2.3. The Pulmonary Extracellular Matrix in Health and Carcinogenesis

The pulmonary ECM plays a decisive role in lung physiology during both development and adult homeostasis. During development, variations in its composition influence lung biomechanics in order to orchestrate various cellular processes, including differentiation and migration. During homeostasis, it maintains tissue architecture, providing mechanical stability and elasticity essential for respiratory function. Recent studies have unveiled the complexity of lung ECM composition, comprising various proteins, glycosaminoglycans, and modifying enzymes, assembling into intricate biomaterials (Burgstaller et al., 2017).

The interstitial lung ECM consists of a loose network primarily composed of collagens, mostly types I and III, along with elastin as key structural proteins (Suki, Ito, Stamenovic, Lutchen, & Ingenito, 2005) (***Figure* , left panel**). These two types of proteins in combination with other ECM components are organized in a manner that imparts softness, elasticity, and resilience to lung tissue, enabling it to stretch and recoil efficiently during breathing (Senior, Bielefeld, & Abensohn, 1975). Enzymatic cross-linking of collagen and elastin, a crucial step during their biosynthesis, is primarily facilitated by enzymes from the lysyl oxidase family (LOX, LOXL1–4) and the transglutaminase family (TG1–7, FXIII-A). This process imparts the ECM components with their characteristic tensile strength (Thomas R Cox et al., 2013; Iismaa, Mearns, Lorand, & Graham, 2009). This composition of the lung ECM is maintained by the activity of resident fibroblasts and contributes to tissue homeostasis. Variations in the collagen content of the parenchyma during development (Tanaka & Ludwig,

1999) or in fibrosis (Dolhnikoff, Mauad, & Ludwig, 1999) have suggested an important role for these protein fibers in shaping the overall function and structure of the lung.

In lung cancer, ECM undergoes profound changes fostering *tumour growth and invasion* (Burgstaller et al., 2017). Fibroblasts are the main architects of ECM in both physiological and pathological states, producing various ECM proteins (Plikus et al., 2021). In particular, cancer-associated fibroblasts (CAFs) are key players in ECM remodelling, as they are responsible for synthesizing and depositing substantial amounts of ECM components (Socovich & Naba, 2019). Collagen, being a major contributor to the tensile strength within lung architecture, plays a decisive role in tumour matrix stiffening. Besides aberrant collagen deposition from CAFs, realignment and alterations in collagen cross-linking have been observed in lung cancer (Pankova et al., 2016). Notably, malignant lung ECM exhibits high levels of hydroxylysine aldehyde-derived collagen cross-links (HLCCs) and lower levels of lysine aldehyde-derived cross-links (LCCs), resulting in increased matrix stiffness (Y. Chen et al., 2015). Additionally, some tumour cells can directly produce high levels of some ECM components such as collagen (Fang et al., 2019) and other ECM-associated proteins (Alexandra Naba et al., 2012), including secreted factors and modulators of the matrix including the LOX family (Hebert et al., 2020). Thus, malignant pulmonary ECM is characterized a denser, more cross-linked, and less porous matrix, resulting in an extensively stiff tumour stroma (Affo, Yu, & Schwabe, 2017; Joshi et al., 2021) (***Figure , centre panel***).

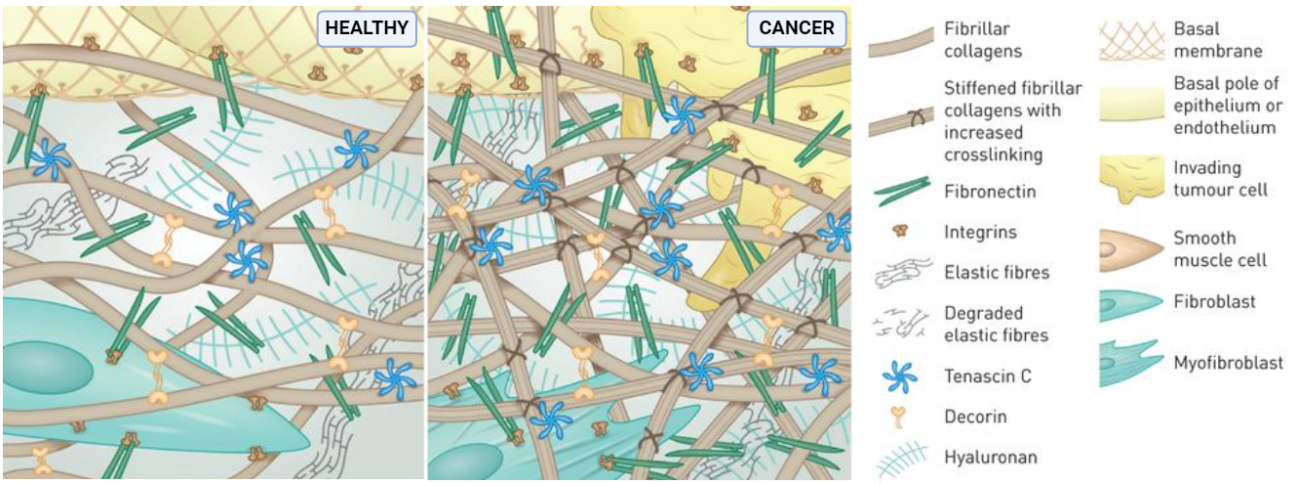

Figure 4. *Differences between healthy and malignant pulmonary extracellular matrix (ECM) [Figure modify from (Burgstaller et al., 2017)].*

1.2.4. Stiffness Sensing

Cells sense ECM stiffness through a process called mechanotransduction, by which mechanical cues from the ECM are converted into biochemical signals within the cell. At the core of this process are the heterodimeric transmembrane receptors integrins (Richard O Hynes, 2002). Integrins play a crucial role in mechanotransduction, acting as the cell's primary sensors. Comprising an α and a β subunit, integrins exist in various combinations, resulting in diverse receptor isoforms and, consequently, a specific repertoire of ligands

(Takada, Ye, & Simon, 2007). The human genome encodes 18 α and 8 β subunits, forming at least 24 unique integrin heterodimers with distinct binding affinities for ECM components such as collagen, and fibronectin (Humphries, Byron, & Humphries, 2006; Hynes, 2004). For instance, α1β1, α2β1, α10β1, and α11β1 are a class of integrins that bind only with GFOGER-like sequences in collagen (Zeltz & Gullberg, 2016). Within the framework of the previously discussed tissue-specific ECM deposition, it is notable that integrins also manifest differential expression profiles among diverse tissues.

Integrin activation is finely regulated by a combination of intracellular activators, such as talins, and kindlins ('inside-out' activation), as well as extracellular matrix ligands like collagen and fibronectin ('outside-in' activation) (Wrighton, 2013). Upon activation, integrins cluster to form focal adhesions, which are multi-protein structures that form mechanical links between the matrix and the actin cytoskeleton (Schwartz, 2010). Notably, it has been observed that variations in ECM stiffness may affect the assembly, binding properties, clustering, and stability of integrins and integrin-based adhesions (Kechagia, Ivaska, & Roca-Cusachs, 2019). On stiffer substrates, cells typically exhibit larger focal adhesions, accompanied by increased actin stress fibres, and increased cell spreading (Ladoux, Mège, & Trepat, 2016; Nishimura & Kaibuchi, 2007).

A multitude of proteins, including paxillin, vinculin and focal adhesion kinase (FAK), are recruited to the integrin cytoplasmic domains in order to form focal adhesions (Zaidel-Bar, Itzkovitz, Ma'ayan, Iyengar, & Geiger, 2007). Through these FA-associated proteins, FAs are linked to stress-fibres, a specialised form of filamentous actin (F-actin) associated with contractile myosin II filaments (Burridge & Guilluy, 2016). Cells adjust their FA strength in response to various chemical or physical stimuli through changes in FA composition and size leading to cytoskeletal rearrangements and actomyosin contractility (D. E. Discher, P. Janmey, & Y. L. Wang, 2005; Gupta, Doss, Lim, Voituriez, & Ladoux, 2016). This intricate orchestration of cytoskeletal dynamics leads to cell migration, through the regulation of Myosin II activity by the RHO–GTPase/RHO-associated protein kinase (ROCK) signalling (Pandya, Orgaz, & Sanz-Moreno, 2017; Pandya, Orgaz, & Sanz-Moreno, 2017; Yamada & Sixt, 2019). Hence, cells have a sophisticated mechanism to sense and respond to the stiffness of their surroundings through their focal adhesions and actomyosin cytoskeleton.

1.3. Directed Cell Migration

Cells undergo directed migration in response to gradients of stimuli in their microenvironment. These stimuli can be diffusible chemical factors (chemotaxis) (Kretschmer & Collado, 1980), ECM-bound chemical cues (haptotaxis) (Carter, 1967), mechanical cues (durotaxis) (Lo, Wang, Dembo, & Wang, 2000), geometric features of substrate (topotaxis) (Park, Kim, & Levchenko, 2018) or electric fields (galvanotaxis) (Mycielska & Djamgoz, 2004). Responding to these stimuli, cells polarize and temporarily move towards a specific direction. Contrastively, homogeneous environments or the absence of a sufficiently strong external gradient to "bias" the direction of cell movement results in a population of cells that migrate in random directions.

Directed cell migration includes cyclical series of four essential sequential steps: 1) protrusion of the leading edge of the cell, 2) adhesion of the leading edge to the extracellular substrate, 3) forward translocation of the

cell body, and 4) retraction of the trailing edge. These processes are activated by internal molecular signalling pathways and guided by external factors (***Figure 3***). Key players in this process are the small GTPases, RhoA, Rac1, and Cdc42, which belong to the Rho family, a subfamily of the Ras superfamily. Firstly, small GTPases, such as Rac1 and Cdc42, drive actin polymerization at the leading edge of the cell, leading to formation of lamellipodia (Itoh et al., 2002). In contrast to lamellipodia, the formation of filopodia at the leading edge is driven by Cdc42-induced actin polymerization (Block et al., 2012).

At the cell's rear, Rho-associated protein kinase (ROCK), a downstream effector of RhoA, activates myosin II via phosphorylation, which leads to increased contractility and disassembly of protrusions (Worthylake & Burridge, 2003). This leads to formation of stress fibers in a force-dependent manner, which promotes retraction by inhibiting protrusion formation (Burridge & Wennerberg, 2004; Chrzanowska-Wodnicka & Burridge, 1996). By coordinating these signalling pathways, cells can achieve the necessary polarity and dynamic changes in the cytoskeleton that allow for effective directional migration. This intricate balance of signalling at both the leading and trailing edges ensures that cells can respond appropriately to external gradients.

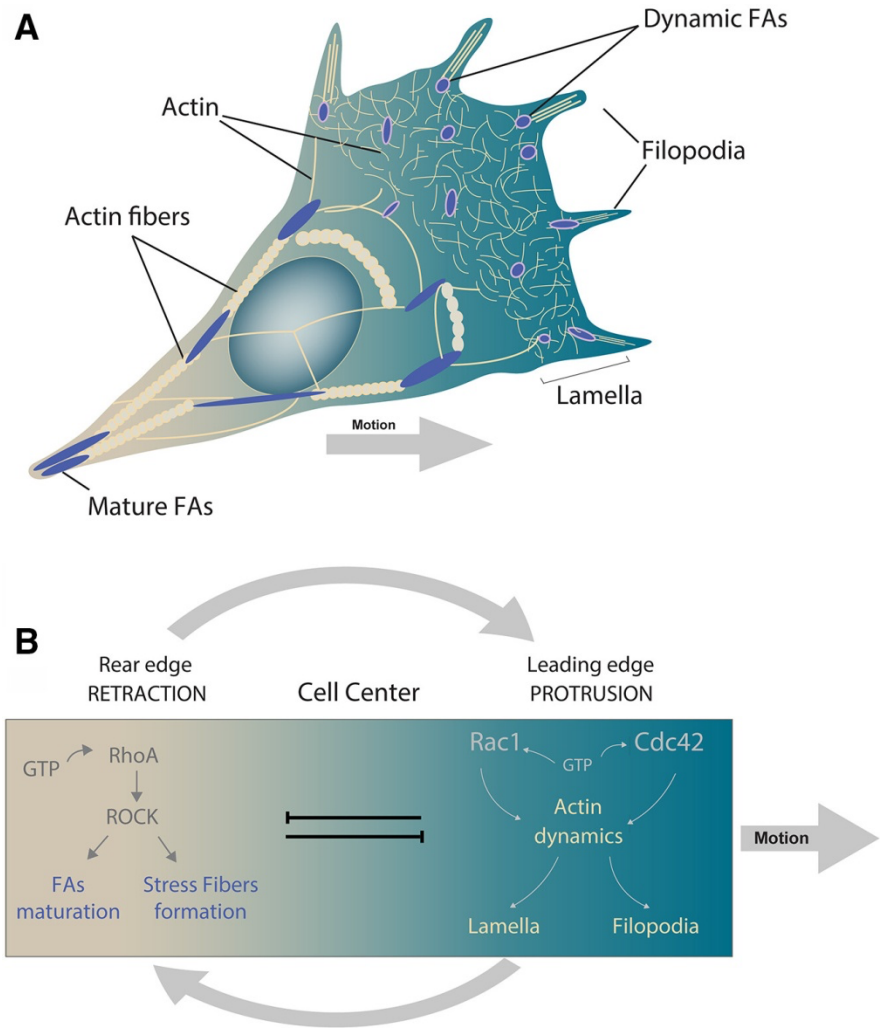

Figure 3. *The establishment of cell polarity and formation of protrusions are essential steps for directed cell migration. A) At the cell' leading edge (front), integrins cluster with each other and other proteins in order to create new focal adhesions (FAs). Large flat projections of cell membrane (lamella) and long thin cytoplasmic protrusions that extend beyond the*

extended lamella (filopodia) are formed. At the cell's rear (back), mature focal adhesions mature and detach from the ECM and actin stress fibers are formed. As a result, cell contracts and migrates. B) At the leading edge, protrusions are formed through the activation of Rac1 and Cdc42 small GTPases, while, at the rear, RhoA/ROCK signalling leads to retraction (Espina, Marchant, & Barriga, 2022).

1.3.1. Durotaxis in Cancer Cells

Durotaxis, the process of cells migrating along stiffness gradients towards stiffer areas, was first identified in fibroblasts two decades ago (Lo et al., 2000). Since then, extensive research in both *in vitro* and *in vivo* models has explored durotaxis in various non-malignant cell types, including smooth muscle cells, immune cells, and stem cells (A. Engler et al., 2004; Christopher D Hartman, Brett C Isenberg, Samantha G Chua, & Joyce Y Wong, 2016; Kang et al., 2024; Lo et al., 2000; Shellard & Mayor, 2021a, 2021b; Vincent, Choi, Alonso-Latorre, Del Álamo, & Engler, 2013). However, the role of matrix stiffness in cancer cell migration remains less well understood. Solid tumours typically exhibit higher stiffness levels than normal tissues, creating a stiffness gradient between the malignant and adjacent healthy tissue (Ishihara & Haga, 2022). Understanding how this gradient influences cancer cell behaviour and migration is crucial.

In cancer research, durotaxis has been observed in a few specific cell lines. These include U87-MG and T98G glioblastoma cells, MDA-MB-231 metastatic epithelial breast cancer cells, and HT1080 fibrosarcoma cells (DuChez, Doyle, Dimitriadis, & Yamada, 2019). Interestingly, a different form of migration, termed "reverse" or "negative durotaxis," where cells move towards softer substrates, has also been reported in HT-1080 cells by another research team (Singh, Schwartz, Lee, Fairbanks, & Anseth, 2014). This behaviour was also later observed in U-251MG glioblastoma and B16 F1 and F10 acral melanoma cell lines (Huang et al., 2022; Aleksi Isomursu et al., 2022). However, the correlation between durotaxis and negative durotaxis remains unclear.

Furthermore, some cancer cell lines exhibit adurotactic behaviour, characterized by a lack of directed migration in response to matrix stiffness. Notable examples include PC-3 prostate cancer cells and NCI-H1299 lung adenocarcinoma cells (Beri et al., 2018; Yeoman et al., 2021). These findings indicate a gap in the research regarding the migratory behaviour of other cancer cell lines, highlighting the need for further investigation.

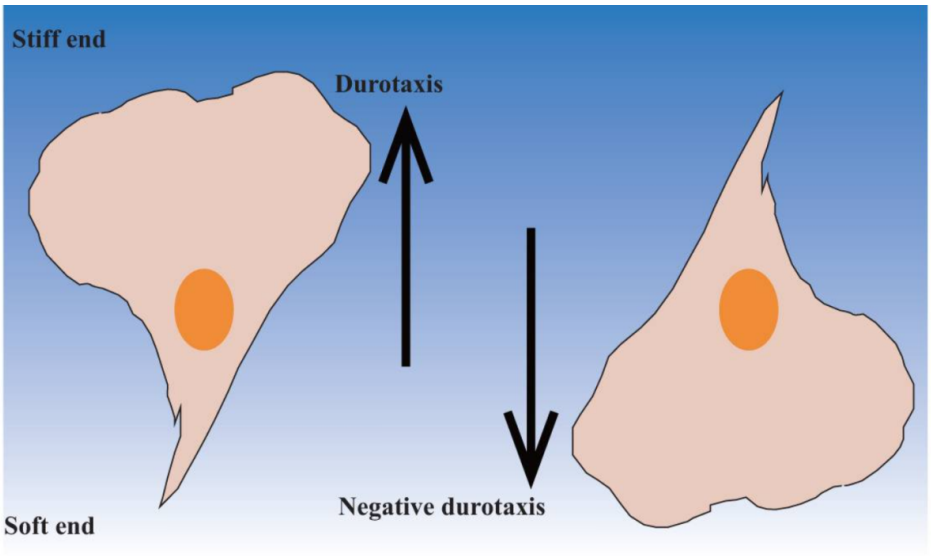

Figure 4. *Durotaxis and negative durotaxis. Left: Durotaxis is the ability of cells to migrate towards stiffer environments of the extracellular matrix. Right: Negative durotaxis is the ability of cells to migrate towards softer environments of the extracellular matrix. [Figure modify from (Ji & Huang, 2023)].*

1.3.2. Mechanisms of Mechanotranduction and Durotaxis

Multiple mechanisms have been investigated to understand their roles in mechanosensing and initiation of durotaxis. Focal adhesions and actomyosin contractility have been linked to ECM rigidity sensing and facilitating durotaxis in several studies (Hoffman, Grashoff, & Schwartz, 2011; A. Isomursu et al., 2022; S. W. Moore, Roca-Cusachs, & Sheetz, 2010; Raab et al., 2012).

Cells exert local traction forces on the ECM through FAs, the main structures connecting the ECM with the actin cytoskeleton. This force transmission varies within different regions of a cell, influencing cell migration. FAs can exist in two states: a stable state with spatially and temporally static traction and a dynamic state where FAs apply fluctuating "tugging" forces to the ECM in a FAK/phospho-paxillin/vinculin-depended manner (Plotnikov, Pasapera, Sabass, & Waterman, 2012). This "tugging" is critical for FAs to sense the local ECM stiffness with high spatial resolution, promoting migration towards stiffer ECM. High-resolution live Traction Force Microscopy (TFM) has shown that on softer substrates, there are more tugging FAs compared to those with stable traction, thereby supporting durotaxis in fibroblasts (Plotnikov et al., 2012).

Additionally, signalling components downstream of FAs transduce external mechanical signals, such as ECM stiffness, to regulate cell polarization and directed migration. Focal adhesion kinase (FAK), one of the first molecules recruited to FAs in response to mechanical stimuli, is crucial for durotaxis (Lachowski et al., 2017; Lachowski et al., 2018). As a key mediator of mechanotransduction, FAK relays these signals to other mechanotransducers within the cytoplasm, such as the Yes-associated protein (YAP). FAK controls the nuclear translocation and activation of YAP and transcriptional co-activator with PDZ-binding motif (TAZ) in response to mechanical activation (Dasgupta & McCollum, 2019). Following changes in cell mechanics, such as cell spreading, YAP and TAZ move to the nucleus to promote the expression of genes involved in motility, apoptosis and proliferation. Although, in hepatic stellate cells, stiffness-induced FAK signalling and YAP

nuclear localization are essential for durotaxis (Lachowski et al., 2018), another study suggests that increased YAP activity promotes negative durotaxis in B16 F1 acral melanoma cell line (Huang et al., 2022). Thus, more extensive studies are needed to determine the exact mechanisms that regulate durotaxis.

Actomyosin-mediated cell contractility is a fundamental element of cell migration and a key regulator of durotaxis (Hakeem et al., 2023). Actin polymerization pushes against the cell edge, while myosin contractility pulls actin filaments away from the edge in a process known as retrograde flow. Myosin II is crucial for cell polarization, with studies showing that this protein is unpolarized on a soft matrix, but repolarizes when cells migrate from softer to stiffer matrices, indicating its role in durotaxis (Raab et al., 2012). Furthermore, filopodia and lamellipodia act as sensors of ECM stiffness through a myosin II-dependent mechanism (Oakes et al., 2018; Wong, Guo, & Wang, 2014).

Actin regulators are also involved in durotaxis. For instance, inhibition of the Arp2/3 complex, which regulates actin filament branching in lamellipodia, prevents positive durotaxis in U87 glioblastoma cells (DuChez et al., 2019), although this mechanism may not be universal, as Arp2/3 inhibition does not affect durotaxis in human retinal pigment epithelial cells (Rong et al., 2021). These interconnected mechanisms and pathways demonstrate the complexity of mechanotransduction and durotaxis, highlighting the importance of more research delving into the mechanisms of stiffness sensing and durotaxis in both health and disease.

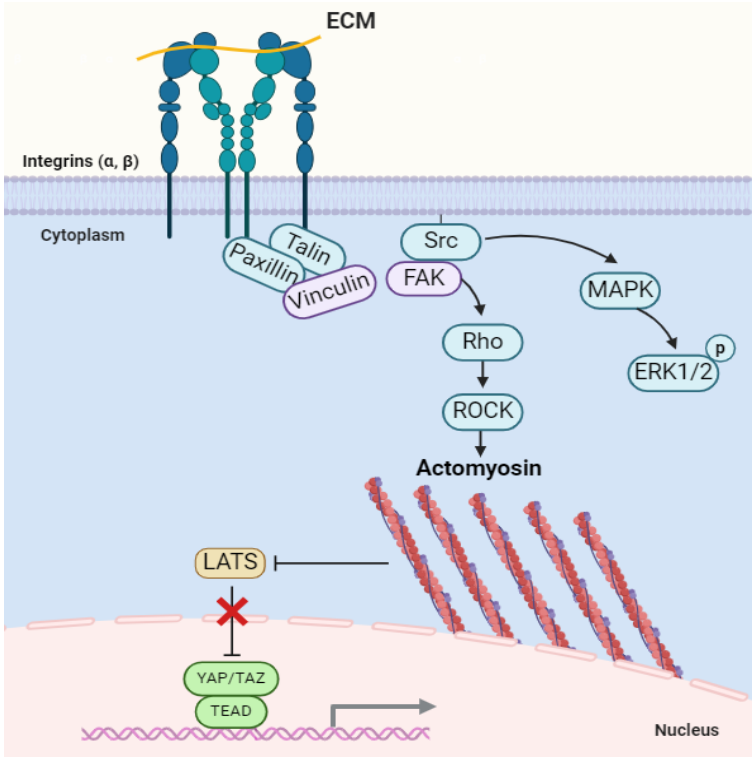

Figure 5. *Key players of integrin mechanosensitive signalling. Integrins cluster to form focal adhesions, dynamic multi-protein complexes that connect the ECM to actin filaments in the cytoskeleton. Focal adhesion kinase (FAK), paxillin, talin, and vinculin are critical for the formation and function of focal adhesions. Integrin activation initiates various signalling pathways, including MAPK/ERK pathway Rho GTPases and YAP/TAZ signalling, resulting in actin-myosin skeleton contractility, spreading, polarization and migration (created using Biorender.com).*

1.4. The Role of Durotaxis in Cancer Metastasis

Directional cell migration is a defining point of embryonic development, homeostasis, and cancer metastasis. Metastasis, one of the main hallmarks of cancer (Hanahan & Weinberg, 2011), is the spread of malignant cells from a primary tumour to distant organs and the primary cause of cancer-related deaths (Dillekås, Rogers, & Straume, 2019). Effective strategies to prevent metastasis would greatly benefit cancer patients. Metastasis is a complex multi-step process known as the metastatic cascade, which includes: 1) local invasion of malignant cells into surrounding tissues, 2) entry into the circulatory and lymphatic systems (intravasation), 3) survival in the circulatory system, 4) exit of circulating tumour cells (CTCs) into adjacent normal tissues (extravasation), and 5) colonization of distant organs (Gerstberger, Jiang, & Ganesh, 2023).

Cancer cell migration is essential for expanding tumour margins and initiating the metastatic cascade. For metastasis to occur, cancer cells must interact with the extracellular matrix (ECM) to invade local tissues. The stiffening of the ECM around tumours creates a stiffness gradient at the tumour-stroma interface, which cancer cells may sense (DuChez et al., 2019). FA-mediated sensing of local stiffness may complement biochemical gradient sensing of diffusible stimuli to refine cell path-finding during the first steps of metastasis. An intriguing study on breast tumour mastectomies revealed that the invasive front of these tumours was stiffer than the rest of the tumour mass (Acerbi et al., 2015).

Durotaxis could enable cancer cells to escape adverse conditions such as hypoxia and necrosis at the primary site. This increased stiffness can facilitate directed and efficient migration away from these hostile environments. Moving towards stiffer areas not only aids in cancer cell escape but also enhances their proliferative capacity and promotes tumour growth, as demonstrated in various studies (Bae et al., 2014; Schrader et al., 2011; Umesh, Rape, Ulrich, & Kumar, 2014). Thus, more research is needed so we can better understand the stiffness landscape of tumours, how cancer cells react to it and how durotaxis contributes to the metastatic potential of cancer cells and possibly develop strategies to mitigate cancer progression.

1.5. Studying Durotaxis *in vitro*

Despite the indispensable role of animal models in cancer research, precisely delineating the impact of individual extracellular matrix (ECM) cues on tumour progression remains challenging (Mak, Evaniew, & Ghert, 2014). Within conventional cell culture, the plastic bottom of a culture dish exhibits a stiffness of approximately 10^7 kPa (GPa), surpassing the stiffness of most tissues in the human body by four orders of magnitude (0.1-1000 kPa) (Yi, Xu, & Liu, 2022). Hence, accurately recapitulating the stiffness of tumour tissue *in vitro* is imperative for establishing physiologically relevant cancer models. Biomaterials have emerged as indispensable tools for mimicking the tumour microenvironment since the early 1980s (Bissell, Hall, & Parry, 1982). Over the past decade, there has been a notable upsurge in the fabrication of artificial 2D or 3D ECM models that faithfully mimic distinct aspects of the tumour ECM, thereby enabling the study of the role of ECM in cancer cell behaviour (Beri et al., 2018; Tang & Liu, 2023).

A diverse range of biomaterials is available for engineering ECM models, with hydrogels emerging as the foremost choice. These hydrophilic networks have been extensively utilized in *in vitro* cell culture systems to examine various facets of cellular behaviour, encompassing proliferation, differentiation, morphology, spreading, and adhesion (Beri et al., 2018; Discher, Mooney, & Zandstra, 2009; Khatiwala, Peyton, & Putnam, 2006; Vining & Mooney, 2017). Hydrogels may be categorized as 2D or 3D and can be composed of natural (e.g., hyaluronic acid, agarose, collagen, or gelatin), synthetic (e.g., Polyethylene glycol (PEG), Polyacrylamide (PA), or Poly(l-lactide) (PLA)), or hybrid materials (M. Chen et al., 2022; Liu & Vunjak-Novakovic, 2016). Each category encompasses a diverse range of hydrogels, and the judicious choice among them is contingent upon the specific demands of the study.

2D polyacrylamide (PA) hydrogels have proven to be effective tools for conducting basic mechanobiological studies (Barber-Pérez et al., 2020; Kaukonen et al., 2016; Tse & Engler, 2010). While 3D hydrogels offer a more faithful representation of the in vivo environment, they are not suitable for in independently examining the role of individual biophysical cues to delineate their specific contributions to cellular processes (Pradhan, Clary, Seliktar, & Lipke, 2017; Wisdom et al., 2018).

For studying durotaxis *in vitro*, the hydrogels utilized must feature a stiffness gradient to observe the cells' bias to migrate toward a particular stiffness value. Numerous methods have been devised to fabricate stiffness gradient hydrogels that faithfully mimic the mechanical heterogeneity observed *in vivo*, each with its own set of advantages and disadvantages (Raimon Sunyer & Trepat, 2020). The most common approach involves polymerizing two adjacent drops containing different concentrations of acrylamide and bis-acrylamide (Barber-Pérez et al., 2020; Koser et al., 2016; Lo et al., 2000). While other methods may offer enhanced precision, they often entail higher costs, labour intensiveness, and time consumption, as well as necessitating specialized equipment or being limited by gel thickness for high-resolution microscopy (Hadden et al., 2017; Hakeem et al., 2023; D. Lee et al., 2019; R. Sunyer, Jin, Nossal, & Sackett, 2012; Raimon Sunyer & Trepat, 2020; Xin, Dai, Gregory, Han, & Alge, 2020).

In this project, we implemented a previous published protocol for generating PA-based hydrogels that exhibit a continuous stiffness gradient from 0.5 kPa to 22 kPa (Barber-Pérez et al., 2020). To mimic the lung ECM, we coated the top of the hydrogels with collagen I, the main protein component of lung ECM (Suki et al., 2005). These hydrogels can be easily and quickly fabricated at a low cost in any laboratory without the need for specific equipment. Additionally, their thin composition allows for high-resolution imaging. A significant feature of this method is the incorporation of fluorescent beads into the hydrogels, with the bead density positively correlating with the gel stiffness. Consequently, stiffness at every point across the gel gradient can be quantified without the need for AFM, only by using an equation that describes the correlation bead density and stiffness.

Motivation and Aims

Mechanobiology has emerged as a captivating realm within cancer biology, offering insights into how cells respond to the stiffness of their environment by modulating morphology, motility, proliferation, and differentiation. Central to numerous biological processes, including development and wound healing, cell migration seems to be particularly sensitive to matrix stiffness, with many cell types exhibiting directed cell migration towards stiffer environments, a process called durotaxis.

Cancer cell migration and metastasis are influenced by various biochemical diffusible factors. However, as many tumour microenvironments gradually stiffen, it would be beneficial to investigate how matrix stiffness affects cancer cell behaviour. Only a handful of studies have explored the influence of ECM stiffness on cancer cells, in which only one cell line is from lung adenocarcinoma (DuChez et al., 2019; Huang et al., 2022; A. Isomursu et al., 2022; Yeoman et al., 2021). Understanding the intricate interplay between extracellular matrix stiffness and the migratory behaviour of cancer cells holds immense promise not only for unravelling mechanisms underlying tumour invasion and metastasis, but it also presents an opportunity to develop interventions to impede tumour progression.

It is well-established that the stiffness of lung tumours is substantially higher than that of normal lung tissue as a result of ECM remodelling through activation of CAFs and extracellular collagen accumulation, crosslinking and fibrosis (Miyazawa et al., 2018). Due to this gradual stiffening of the tumour microenvironment, we hypothesized that durotaxis might also govern migration of cancer cells.

This thesis seeks to delve into the impact of matrix stiffness on the migratory behaviour of lung cancer cells *in vitro*. The **primary objective** is to explore how matrix stiffness impacts the migratory patterns of lung cancer cells, providing insight into the role of stiffness in tumour metastasis. To achieve this goal, EGFR-driven NSCLC cell lines will be seeded onto continuous stiffness gradient polyacrylamide hydrogels spanning a stiffness range of 0.5 to 22 kPa (Barber-Pérez et al., 2020). This range of stiffness values mimics the conditions encountered by cells in both healthy and malignant lung tissues. The protocol that we will use offers an indirect method to measure local stiffness at every point of the hydrogel, without the need of AFM. The hydrogel will be characterized and divided into three distinct zones with varying stiffness ranges to obtain more precise information about the migratory behaviour of lung cancer cells.

Live-cell imaging will be utilized to record the migration patterns of each cell line. The trajectories of individual cells will be analyzed to determine if they exhibit directed migration across the gradient towards stiffer regions (durotaxis), softer regions (negative durotaxis), or if they migrate randomly regardless of stiffness (adurotaxis). To validate these observations, cells seeded on stiffness gradient hydrogels will be fixed at 0 and 24 hours post-seeding. Subsequent nuclear staining will enable the measurement of cell distribution and density across the gradient at each time point.

The **second aim** of this thesis is to explore the overall impact of ECM stiffness on the migratory behaviour and motility of lung cancer cells. This will be accomplished by measuring additional migration parameters, including cell speed and distance travelled. By analyzing these parameters, we aim to gain deeper insights

into how varying ECM stiffness influences cancer cell movement and how this might connect to their metastatic potential.

Finally, this project aims to explore any changes in actin cytoskeleton changes across the stiffness gradient. The morphology, i.e. cell area and circularity, of lung cancer cells will be assessed through actin cytoskeleton staining and high-resolution microscopy will facilitate visualization of their morphology at various locations across the stiffness gradient.

By delving into these aspects, this study seeks to elucidate the effects of matrix stiffness on the migratory behaviour of lung adenocarcinoma cells, offering an indication of how ECM stiffness contributes to lung cancer metastasis.

3. Materials and Methods

3.1. Cell Culture and Sub-culturing

Four EGFR-driven NSCLC cell lines were cultured in RPMI (Sigma, cat. no. R8758-500ML), supplemented with 10% Fetal Bovine Serum (FBS) (Biowest, cat. no. S181B-500), 1% Penicillin-Streptomycin (Biowest, cat. no. L0022-100) and 2mM L-Glutamine (Biowest, cat. no. X0550-100). Information for each cell line is shown in ***Table 1*** and their oncogenic mutations are shown in ***Table 2***. The cells were tested for mycoplasma contamination and cultured at +37°C, 5% CO_2 in a humidified incubator. For sub-culturing, cells at 80-90% confluency were washed once with phosphate-buffered saline (PBS) followed by detachment from the plate surface via 1x Trypsin.

Cell line(s)	Patient description	NSCLC subtype	Primary/metastasis
HCC-827	Female, 39 years old	Adenocarcinoma (LUAD)	Primary
NCI-H2279	Female, 52 years old	Adenocarcinoma (LUAD)	Primary
HCC-4006	Male	Adenocarcinoma (LUAD)	Metastasis (from pleural effusion)
PC9	Male	Adenocarcinoma (LUAD)	Primary

Table 1. *Cell lines used in the following experiments (Information obtained from cbioportal).*

Cell line(s)	EGFR	TP53
HCC-827	E746_A750del	V218del
NCI-H2279	E746_A750del	Y234C
HCC-4006	F295Lfs*39	Y205H
PC9	E746_A750del	R248Q

Table 2. *Oncogenic mutations of each cell line (Information obtained from cbioportal).*

3.2. Cryopreservation and Deep Freezing of Cells

For the cryopreservation of cells, cells reaching 50-60% confluency were gently detached from the plate via Trypsin-EDTA and resuspended in PBS. The resulting cell suspensions were then transferred to 15 ml conical tubes and centrifuged at 1500 rpm for 10 minutes. Subsequently, the cell pellets were resuspended in freezing medium, constituting of 90% fetal bovine serum (FBS) and 10% dimethyl sulfoxide (DMSO), transferred into cryovials and stored in liquid nitrogen tanks.

3.3. Fabrication of Continuous Stiffness Gradient Polyacrylamide Hydrogels

For the generation of stiffness gradient polyacrylamide hydrogels, a previously published standardized protocol was implemented (Barber-Pérez et al., 2020). These hydrogels are designed to exhibit a continuous stiffness gradient ranging from 0.5 to 22 kPa – the range of physiological stiffness encountered by cells across

many tissues. Initially, 35 mm glass-bottom dishes (Cellvis, D35-14-1-N) or 24-well glass bottom plates (Cellvis, P24-1.5H-N) were treated with Bind-Silane solution for 30 minutes at room temperature in order to promote hydrogel attachment to the glass bottom surface. This solution contains 3-(Trimethoxysilyl)propyl methacrylate (Thermo Scientific, cat. no. 216555000), acetic acid and absolute ethanol (96% in volume). After Bind-Silane was aspirated, the glass was washed twice with absolute ethanol (96% in volume) and left to dry.

For the preparation of hydrogels, 40% (w/v) acrylamide (Sigma-Aldrich, A4058) and 2% (w/v) N,N-methylene-bis-acrylamide (Thermo scientific, J63265.AP) were mixed with PBS and vortexed. In order to get a stiffness gradient spanning from 0.5 to 22 kPa, two different pre-polymer solutions corresponding to Young's moduli equal to 0.5 and 22 kPa were prepared as a result of different ratios of acrylamide and bis-acrylamide (Table 3). A key point of this preparation is the incorporation of fluorescent beads into the 22 kPa acrylamide pre-polymer solution before polymerization. The density of these beads across the hydrogel offers an indirect measure as readout for stiffness without the need for Atomic Force Microscopy (AFM). Briefly, 0.1 μm fluorescent yellow-green (505/515) microspheres (~1.2 × 10^{11} ml^{-1} final concentration, Invitrogen, F8803) were added to the 22 kPa solution. Before use, sonication of beads for 3 minutes was performed to avoid bead aggregation. During the whole process of preparing the pre-polymer solutions, the solutions were kept on ice to avoid fast polymerization.

40% Acrylamide (μl)	Acrylamide %	2% Bis-Acrylamide (μl)	Bis-Acrylamide %	PBS (μl)	Young's Modulus (~kPa)
63	**5**	**10**	**0.04**	**397**	**0.5**
150	**12**	**50**	**0.2**	**300**	**22**

Table 3. *Relative acrylamide and bis-acrylamide concentrations for the fabrication of the soft and stiff pre-polymer solutions.*

Polymerization of polyacrylamide solutions was initiated by the addition of N,N,N′,N′-tetramethylethylenediamine (TEMED) (0.2% by volume, Thermo Fisher Bioreagents, BP150-100) and 10% ammonium persulfate (APS) (0.1% by volume, Thermo Fisher Bioreagents, 327081000) to the solution. Immediately afterwards, the two polymerizing solutions were quickly vortexed and a 7.8 μl droplet of each one was pipetted on top of the glass bottom surface, as it is shown in *Figure 6*. A 13 mm circular coverslip was placed on top of the drops, allowing the two droplets to diffuse together. As a result, a continuous stiffness gradient across the hydrogel was achieved, where the stiff region displayed the highest bead density. The hydrogels were left to polymerize for 1-2 hours at room temperature protected from light. Then, the gel was immersed in PBS for 5 minutes. The coverslip was gently removed with medical tweezers and a bent needle and the gel was washed twice with PBS to remove any excess acrylamide.

Subsequently, a solution of 1 mg ml^{-1} Sulfo-SANPAH (Sigma-Aldrich, 803332) and 2 mg ml^{-1} N-(3-dimethylaminopropyl)-N′-ethylcarbodiimide hydrochloride (EDC) (Sigma-Aldrich, E7750) in 50 mM 2-[4-(2-hydroxyethyl)piperazin-1-yl]ethane-1-sulfonic acid (HEPES) (Thermo Fisher Bioreagents, 172570250) was added on top of the hydrogels and incubated for 30 min at room temperature, protected from light and subjected to gentle agitation. The gel and solution were then ultraviolet (UV) irradiated for 10 minutes to

activate the Sulfo-SANPAH, and the plate was washed with PBS three times to remove any residual compounds. Finally, hydrogels were coated with 9.2 µg ml^{-1} collagen type I solution overnight at +4 °C for cells to adhere.

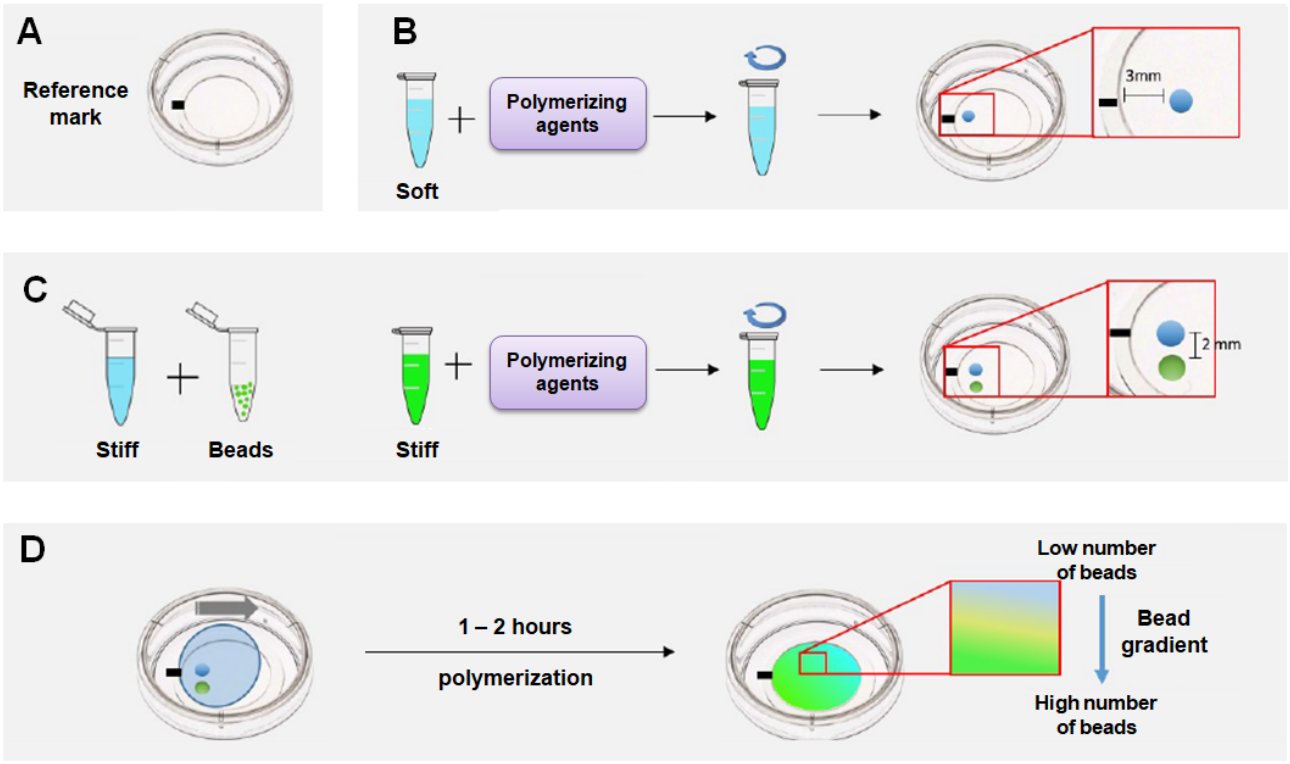

Figure 6. *Scheme for the fabrication of stiffness gradient PA hydrogels. A) A reference mark is drawn on the glass-bottom dish to locate the gradient within the gel. B,C) Soft and stiff pre-polymer solutions with different concentrations of acrylamide and bis-acrylamide are prepared. Fluorescent beads are added only to the stiff pre-mix. After vortexing both pre-mixes, polymerizing agents (APS and TEMED) are added and, quickly after, one droplet of each solution is put onto the glass-bottom dish, as indicated. During all steps before polymerization, the solutions are kept on ice. The droplets are pipetted on top of the dish in room temperature (RT) D) A coverslip is placed on top of them in the specific mode indicated. After 1-2 hours polymerization, the coverslip is removed and a gradient of beads and stiffness is yielded [Figure modify from (Barber-Pérez et al., 2020)].*

3.4. Cell Seeding on Hydrogels

Collagen solution was removed and gels were gently washed once with phosphate-buffered saline (PBS). The uniform distribution of cells across the hydrogel was visually confirmed using bright-field microscopy prior to any experimental procedure.

3.5. Immunostaining

Cells were fixed with 4% paraformaldehyde (PFA) for 15 minutes at RT. PFA was aspirated and cells underwent gentle washing thrice with PBS. Cells were blocked with 5% bovine serum albumin (BSA) in PBST (PBS with 0.1% TritonX) for 30 minutes at RT. Subsequently, cells were incubated with a primary antibody for 1 hour at RT, followed by four PBS washes. Hoechst (1:1000) and Phalloidin (1:200) stains were introduced into the secondary antibody mixture at this stage. After the incubation, cells were washed four times with PBS. Finally, cells were kept either with PBS or were mounted and stored in the refrigerator (4°C) until imaged.

3.6. Cell Tracking and Time-lapse Movies Analysis

For the analysis of cell migration, live-cell imaging on continuous 0.5–22.0 kPa stiffness gradient polyacrylamide hydrogels was performed over a time period of 12 hours. Cells were seeded and allowed to settle in the incubator for 1 hour before imaging. Each hydrogel was divided into three regions that we defined as soft, intermediate, and stiff depending on the fluorescence of each region. The soft region displayed a mild gradient from none to mild fluorescence, the intermediate from mild to intense fluorescence, and the stiff region had almost uniform intense fluorescence (*Figure 7A*). Cell movement was recorded in each region at 30 minutes intervals using the IncuCyte ZOOM and time-lapse movies were acquired.

Cell tracking was performed using the Manual Tracking plug-in of the ImageJ software (*Figure 7B*). Single cells across the gradient were tracked through time and their trajectories were recorded and saved in a .txt file. We focused on single, individual migrating cells to be able to evaluate durotaxis independent of cell-cell contact. Mitotic, dying or crowded cells were excluded from the analysis. The resulting .txt file was directly imported into the Chemotaxis and Migration Tool software V2.0 (Ibidi) for further analysis.

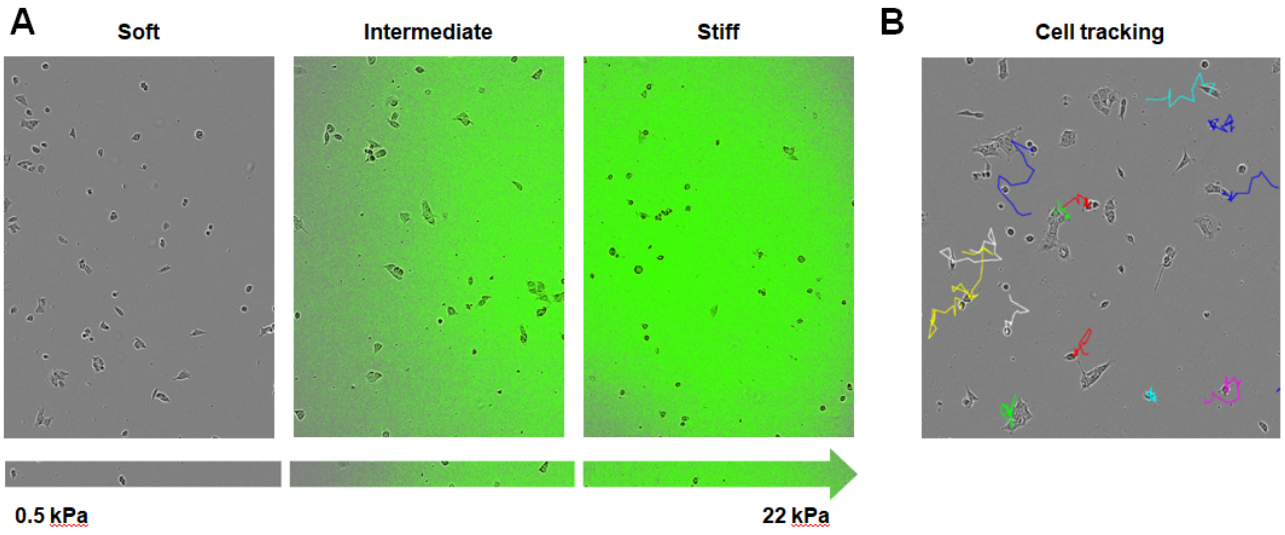

Figure 7. *Procedure of cell tracking. A) Example images from IncuCyte ZOOM of the three regions (soft, intermediate, stiff) of the stiffness gradient hydrogels. Due to the fluorescent beads added in the stiff pre-solution, hydrogel stiffness*

correlates with the green fluorescence of each region. B) Recorded cell paths using the Manual Tracking plug-in from ImageJ Fiji.

3.6.1. Trajectory Plots

Trajectory plots were obtained from Chemotaxis and Migration Tool software V2.0 (Ibidi) for the illustration of the movement patterns of lung cancer cells over time. Typically, these plots were generated using the IncuCyte ZOOM time-lapse microscopy data, where cell positions were recorded at every 30 minutes intervals, and ImageJ software was employed to connect these positions into continuous paths. Each trajectory represents the path taken by an individual cell as it migrates across the stiffness gradient.

In a trajectory plot, all (x, y) coordinates of the cells' starting points are set to (0,0) using a coordinate transformation. Furthermore, the centre of mass, which is shown in trajectory plots, represents the average of all single cell endpoints. Its x and y values indicate the direction, in which the group of cells primarily travelled. Thus, the general direction of cell migration is displayed and allows for first data interpretations.

3.6.2. Angular Displacement Rose Plots

Angular displacement in the context of cell migration refers to the change in direction of movement of a migrating cell over time. It quantifies how much the cell has turned or changed its orientation relative to its previous direction of movement. It is calculated based on the initial and final position of each cell and shows the angle through which each cell migrates and the direction of each path. Angular displacement was calculated separately for each cell that was analyzed, and then all cell values were averaged. To see if a cell population undergoes directional migration, the uniformity of migration is statistically evaluated with Rayleigh test on the angular displacement data (B. R. MOORE, 1980). Uniformity of cell migration is the null hypothesis and a p-value ≤ 0.05 is considered statistically significant.

Angular displacement data were represented in a rose plot (also known as a circular histogram), which provides a concise visual representation of how cells migrate directionally over time, highlighting any preferred directions or patterns in their movement behaviour. This plot has a circle divided into sectors or “petals”, each representing a range of angles (typically 0 to 360 degrees). The length of each sector represents the proportion of cell movements that fall within that angular range. The different lengths of the sectors create direction peaks, which represent preferred directions or biases in cell migration. On the other hand, an equal length of sectors directed towards every direction indicates random movement, where cells are not biased towards any particular direction.

3.6.3. Forward Migration Index

Another important measure of directed migration is the forward migration index (FMI), which represents the efficiency of the forward migration of cells. FMI is used to measure the displacement of a cell relative to the cell's total path length. For FMI calculation, it is necessary to define the direction of the x-axis and the y-axis in relation to the gradient. Here, we define the x-axis as parallel to the gradient ($\perp$) and the y-axis as perpendicular to the gradient ($\parallel$). We calculated xFMI, which describes the forward migration of cells in a direction parallel to the gradient, and yFMI, which describes the forward migration of cells in a direction perpendicular to the gradient. xFMI and yFMI were calculated separately for each cell that was analyzed, and then all cell values were averaged. To determine if directed cell migration occurred, we compared the xFMI and yFMI values. The larger the xFMI, the stronger the durotactic effect is.

3.6.4. Speed and Distance Migrated

Speed, also called as mean velocity, was calculated as well with Chemotaxis and Migration Tool V2.0. as the sum of individual displacements divided by total time.

3.7. Image Processing and Analysis

3.7.1. Stiffness Characterization

After image acquisition of cell cytoskeleton, hydrogel stiffness right underneath each cell was measured using a previous published indirect method (Barber-Pérez et al., 2020). This method allows inferring the hydrogel stiffness without the need of using Atomic Force Microscopy (AFM). Specifically, the corresponding stiffness of a certain region of the hydrogel can be found by the calculation of the density of fluorescent microspheres in that specific location.

Image acquisition of the fluorescent beads was done using the Nikon AX microscope, equipped with a 40X water objective lens (Apo LWD 40x WI λS DIC N2) and a 488 nm laser line (505/544 nm emission filter). Nyquist tool was adjusted at 3,5 nm zoom. Each acquired image was 122,88 µm (X) x 122,88 µm (Y) x 7 µm(Z) in size, had 6 Z-stacks and the Z upper limit for the acquisition of each stack was about 1 µm underneath the gel surface to avoid capturing any imperfection from the upper layer of the gel.

Subsequently, the resulting images were processed with ImageJ, Fiji software (Schindelin et al., 2012). Initially, maximum intensity projection was applied to the images to enhance fluorescent bead visibility. Subsequently, the threshold input value tool was utilized for the segmentation of beads. The threshold was determined carefully via visual inspection of segmented beads. This threshold may vary considerably between

different hydrogels. Subsequent quantification of segmented beads was achieved using the "Analyse particles" tool in Fiji, with a minimum size criterion set to exclude really small objects, thereby minimizing noise and averting potential overestimation of bead numbers. Bead density was computed by dividing the number of beads by the area unit ($1/10^4$ μm^2) for each image. Finally, stiffness was calculated according to an equation of a correlation curve between bead density and stiffness (Barber-Pérez et al., 2020).

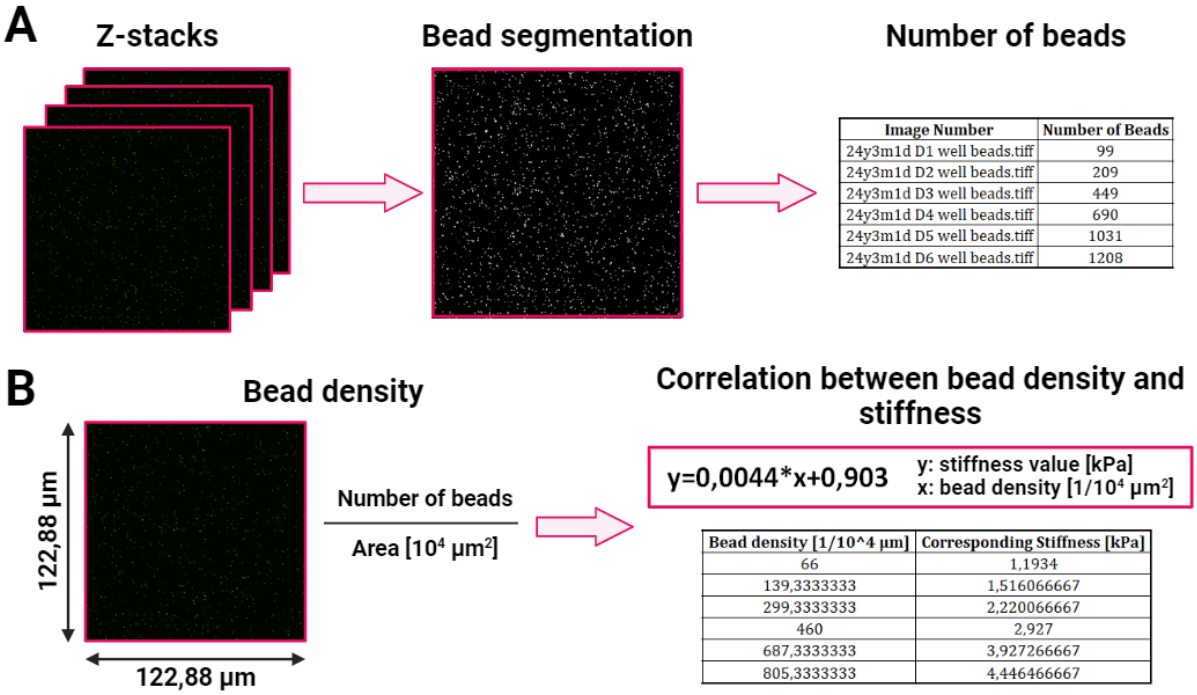

Image Number	Number of Beads
24y3m1d D1 well beads.tiff	99
24y3m1d D2 well beads.tiff	209
24y3m1d D3 well beads.tiff	449
24y3m1d D4 well beads.tiff	690
24y3m1d D5 well beads.tiff	1031
24y3m1d D6 well beads.tiff	1208

Bead density [1/10^4 µm]	Corresponding Stiffness [kPa]
66	1,1934
139,3333333	1,516066667
299,3333333	2,220066667
460	2,927
687,3333333	3,927266667
805,3333333	4,446466667

Figure 8. *Hydrogel stiffness characterization via the calculation of fluorescent bead density. A) The acquired Z-stacks undergo maximum intensity projection, segmentation of beads is conducted in order quantify the beads. B) After bead quantification, bead density is calculated by dividing the number of beads to image area [10^4 μm^2]. After that, stiffness value is calculated by a previously published equation of correlation between bead density and stiffness, represented as y = 0.0044*x + 0.903, where y denotes the stiffness value and x represents the bead density.*

3.7.2. Cell Area and Circularity

Cell area (μm^2) and circularity (a.u.) were calculated using the ImageJ, Fiji software (Schindelin et al., 2012). Cells seeded on stiffness gradient polyacrylamide hydrogels underwent immunostaining with the actin cytoskeleton stain phalloidin. Image acquisition of single cells on various random locations across the gradient was done using the Nikon AX microscope. Specifically, a 40X water objective lens (Apo LWD 40x WI λS DIC N2) with 594 nm (600/712 nm emission filter) and 342 nm (429/474 nm emission filter) laser lines was utilized. Nyquist tool was adjusted at 3.5 nm zoom. Z-stacks of cells' cytoskeleton were acquired and maximum intensity projection was applied on. The threshold input value tool was utilized for the segmentation of the whole cell periphery. The wand tracing tool was used to select the cells' periphery and ROI manager tool in order add labels on each cell in the image and measure cell area and perimeter. An .xlsx file with this information was exerted. The circularity of the cell was calculated by the operation 4π*area/(perimeter)^2,

where a value of 1 indicates a perfect circle. As the value approaches 0, it indicates an increasingly elongated shape.

3.7.3. Cell Quantification Across the Stiffness Gradient

To quantify cell distribution across the 0.5-22 kPa stiffness gradient, hexbin plots were employed. For their generation, 4 mm x 4 mm tile scans of the gradient surface of each hydrogel were acquired, with the gradient oriented parallel to the x-axis of the tile scan. Tile-scan acquisition was performed using the Nikon AX microscope, equipped with a 20X air objective lens (PLAN Apo λD 20x OFN25 DIC N2), a 405 nm laser line (429/474 nm emission filter), along with a 488 nm laser line (505/544 nm emission filter).

Hexbin plots provide a two-dimensional representation of cell density, facilitating the visualization of spatial distribution patterns. The x- and y-axes represent the 4 mm x 4 mm surface of the hydrogel, encompassing the stiffness gradient. A colour-bar spanning from dark blue to yellow denotes the cell count. Hexagonal bins aggregate the data points, allowing for efficient handling of large datasets and highlighting regions of high cell density. This method ensures an accurate depiction of cell clustering and distribution, offering insights into how cells respond to changes in substrate stiffness.

```
# Step 1: Upload the Excel files
from google.colab import
uploaded = files.upload()

# Step 2: Import necessary libraries
import pandas as pd
import matplotlib.pyplot as plt
import seaborn as sns

# Step 3: Load the Excel files into DataFrames
df1 = pd.read_excel('HCC-827 0 hours.xlsx')
df2 = pd.read_excel('HCC-827 24 hours.xlsx')


# Step 4: Find the common colour scale
plt.figure()
hb1 = plt.hexbin(x1, y1, gridsize=14, cmap='viridis')
hb2 = plt.hexbin(x2, y2, gridsize=14, cmap='viridis')
max_count = max(hb1.get_array().max(),
hb2.get_array().max())
plt.close()
```

```
# Step 5: Create hexbin plots with common colour scale
fig, axs = plt.subplots(1, 2, figsize=(24, 6))

hb1 = axs[0].hexbin(x1, y1, gridsize=12, cmap='viridis', vmin=0,
vmax=max_count)
axs[0].set_xlabel('x-coordinate [mm]')
axs[0].set_ylabel('y-coordinate [mm]')
axs[0].set_title('0 hours')

hb2 = axs[1].hexbin(x2, y2, gridsize=12, cmap='viridis', vmin=0,
vmax=max_count)
axs[1].set_xlabel('x-coordinate [mm]')
axs[1].set_ylabel('y-coordinate [mm]')
axs[1].set_title('24 hours')

#Step 6: Add a common colourbar
cb = fig.colorbar(hb1, ax=axs, orientation='horizontal',
fraction=0.02, pad=0.1)
cb.set_label('Cell count')

plt.show()
```

Figure 9. *Analytical steps and python code for the creation of hexbin plots that represent the number of cells across the stiffness gradient at 0 and 24 hours post-seeding.*

3.8. Statistical Analysis

Statistical analyses and plotting were performed using GraphPad Prism v5 and Chemotaxis and Migration Tool software V2.0 (Ibidi). Angular displacement data were evaluated by Rayleigh test. FMIs were analyzed

by Wilcoxon signed rank test. Cell density was analysed by Kruskal-Wallis one-way ANOVA and Dunn's post hoc test. Speed of cell movement and distance migrated were evaluated by one-way ANOVA and Tukey's post hoc test (***$p \leq 0.001$).

4. Results

4.1. Characterization of Stiffness Gradient Polyacrylamide Hydrogels

Polyacrylamide hydrogels with a stiffness gradient ranging from ~0.5 kPa to 22 kPa – a range representative of both physiological and malignant lung tissue stiffness – were fabricated according to a previously published protocol (Barber-Pérez et al., 2020). To mimic the lung ECM, we coated the top of the hydrogels with collagen I, the main protein component of lung ECM (Suki et al., 2005). A key step in this protocol involves incorporating fluorescent beads into the polyacrylamide pre-mixture, thereby creating a bead gradient that corresponds with the stiffness gradient (*see section 3.3. Fabrication of Continuous Stiffness Gradient Polyacrylamide Hydrogels for details*). Stiffness at every point across the gel gradient can be quantified without the need for AFM, only by using an equation that describes the correlation bead density and stiffness.

This process results in a round hydrogel with a diameter of 14 mm, featuring a progressively increasing stiffness gradient from the left side to the right. The hydrogel comprises two large areas on its left and right sides, displaying uniform stiffness values of 0.5 kPa and 22 kPa, respectively. Between these areas lies a smaller middle region, approximately 2-4 mm wide, where the bead gradient is present. Consequently, the gradient region occupies a relatively small portion of the total gel area.

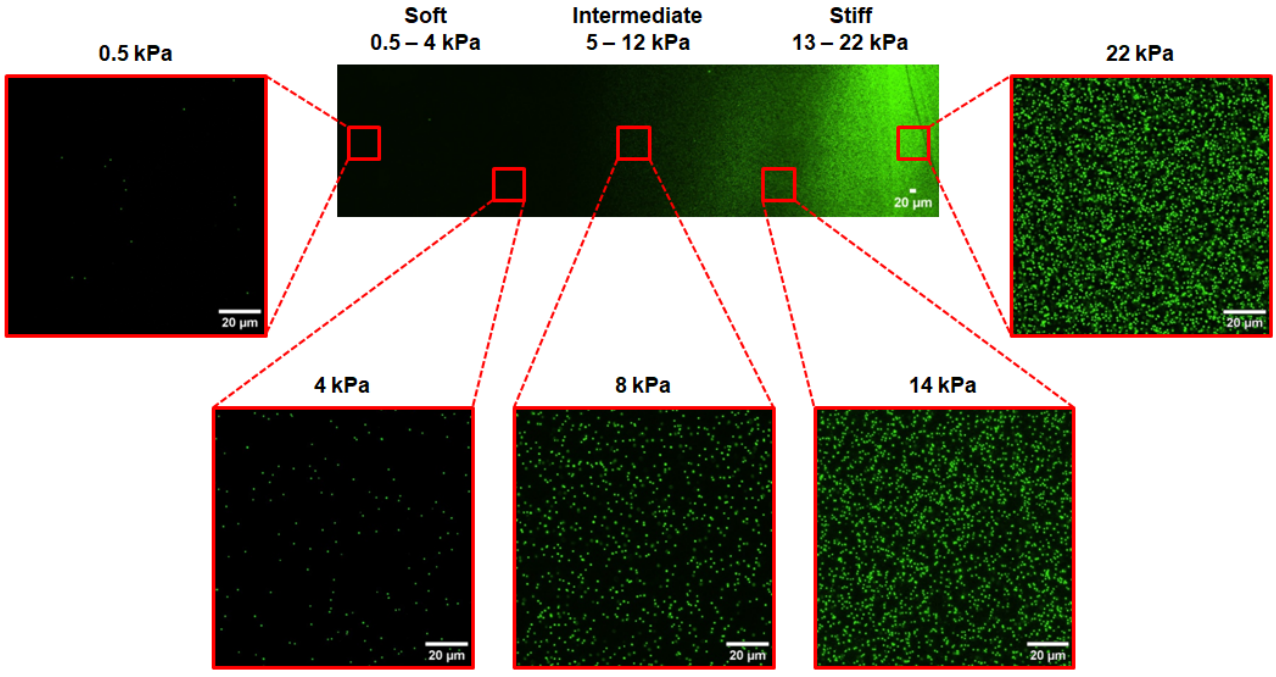

Figure 10. *Distribution of fluorescent beads within the gradient hydrogels. Real tile scan example of the middle region of the hydrogel, where the gradient of beads is located, and the three distinct regions of stiffness range. Close-up images of the beads from different locations across the gradient and their corresponding stiffness value are shown.*

Following this observation, we focused on the 4 mm wide middle part of the gel, where the stiffness gradient exists. Within this region, the hydrogels exhibit a distribution of beads with three differentiated zones: a region with no beads or a very low quantity of beads on the left side of the hydrogel; a region with a gradient of mild to intense fluorescence in the middle part of the gel; and a region with the highest fluorescence of beads on the right side of the gel. We designated these three distinct zones as soft, intermediate, and stiff.

To characterize the stiffness range of each of these zones, we acquired 12 close-up images of the fluorescent beads, capturing adjacent areas from the left corner of the soft zone to the right corner of the stiff zone. The stiffness value at each location was then calculated based on a bead density and stiffness correlation equation described in section *3.7.1. Stiffness Characterization*. Our findings indicated that the soft zone displayed an approximate stiffness range from 0.5 kPa to 3-4 kPa, the intermediate zone ranged from 4-5 kPa to 11-12 kPa, and the stiff zone ranged from 13-22 kPa. These values were consistent across three different hydrogels, with slight variations of 0.5-1 kPa higher or lower.

4.2. Lung Adenocarcinoma Cells Respond to Matrix Stiffness

The primary objective of this study was to investigate whether lung cancer cells exhibit sense and respond to substrate stiffness. To achieve this, we seeded lung cancer cells on collagen-coated polyacrylamide hydrogels featuring a continuous stiffness gradient from 0.5 kPa to 22 kPa. By employing different EGFR-driven NSCLC cell lines, we sought to determine whether matrix stiffness exerts a consistent effect across these seemingly homogeneous groups or if their responses vary.

Live-cell imaging was conducted over a period of 8-12 hours, and single-cell tracking was performed across the three distinct regions of the hydrogel (soft, intermediate, and stiff) (***Figure 11A***). Trajectory plots, visualizing the paths taken by individual cells, were generated for each region, providing an initial impression of whether the cells exhibit a preferential migration towards areas of differing stiffness, thereby indicating a directional bias. Additionally, analyzing the shapes and lengths of the trajectories offered insights into variations in cell behaviour, such as migration distance.

Our findings indicate that HCC-827 cells exhibit a mild tendency to migrate towards stiffer regions in both the soft and intermediate stiffness gradient areas (***Figure 11B***). Specifically, the centre of mass, representing the average of all single cell endpoints, is slightly shifted to the right. In contrast, in the stiff region, the centre of mass is located very close to the origin (0,0), suggesting random movement. Despite these observations, cell tracks in all three regions were oriented almost equally in all directions, indicating weak directional bias.

Furthermore, the migration distance of HCC-827 cells was found to be influenced by substrate stiffness. In the soft region of the stiffness gradient, these cells exhibited extremely low motility with short migration distances. Conversely, in the intermediate and stiff regions, the cells demonstrated significantly higher motility and migrated over longer distances.

NCI-H2279 cells also exhibited a mild tendency to migrate towards stiffer areas across all three regions of the stiffness gradient, as indicated by the centre of mass being slightly shifted to the right in each region (***Figure 12****Figure 12****A***). Despite that, cell tracks in all three regions were oriented almost equally in all directions, indicating weak directional bias. Similar to the behaviour of HCC-827 cells, NCI-H2279 cells demonstrated lower motility and shorter migration distances in the soft region, with displacement increasing in the intermediate region and becoming even more pronounced in the stiff region.

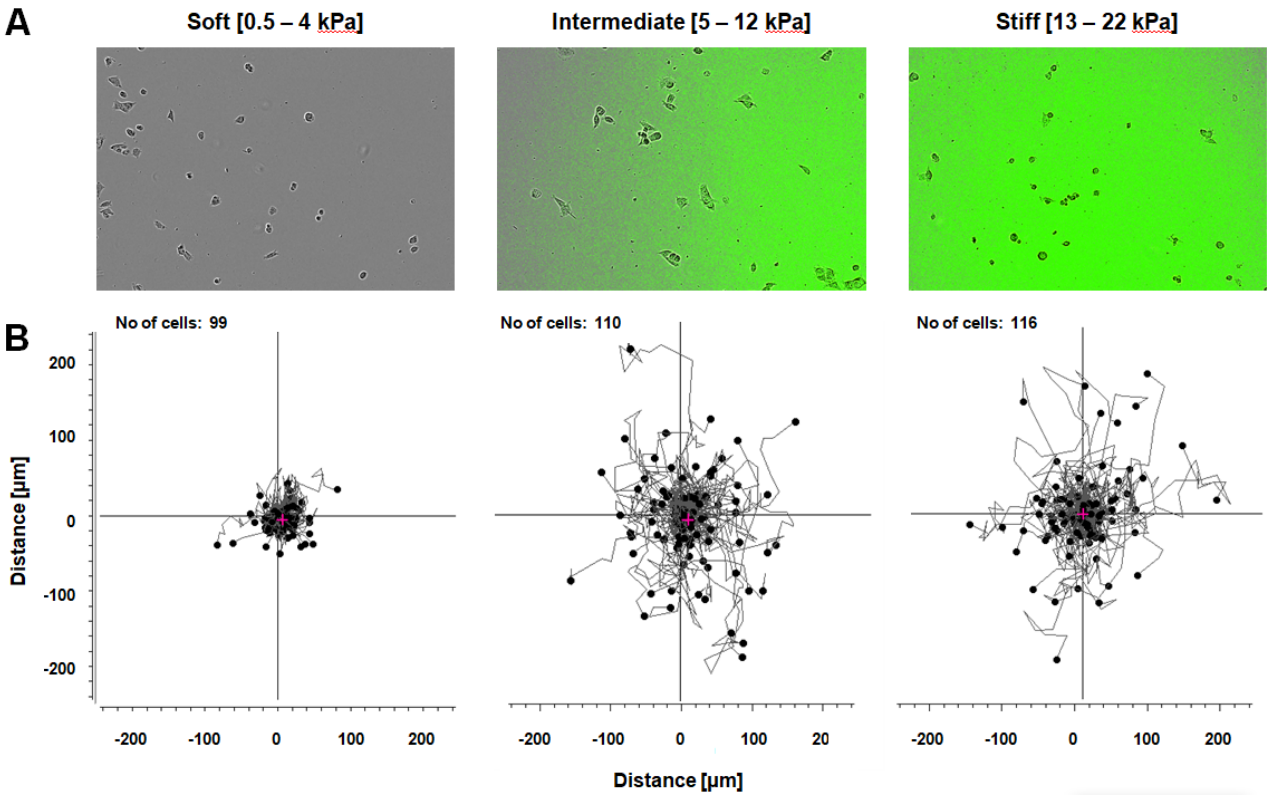

Figure 11. *Live-cell imaging and HCC-827 cell tracking. A) Example images from IncuCyte ZOOM of HCC-827 cells seeded on top of the three regions (soft, intermediate, stiff) of the stiffness gradient hydrogels. B) Trajectory plots of HCC-827 cells seeded on 0.5-22 kPa stiffness gradient. Tracks from individual cells are shown on the soft (left), intermediate (centre), stiff (right) regions. The centre of mass is highlighted by a pink (+), n = 99–116 cells from three independent experiments.*

HCC-4006 cells, on the other hand, exhibited a strong tendency for directed migration, with the majority of cell tracks and the center of mass consistently oriented towards stiffer areas across all three regions of the stiffness gradient (***Figure 12B***). In contrast to HCC-827 and NCI-H2279 cells, the migration distance of HCC-4006 cells varied only slightly between the three regions, indicating persistent movement.

PC-9 cells exhibited a unique migratory behaviour across the three regions (***Figure 12C***). In the soft region, they showed a mild tendency to migrate towards stiffer areas, as indicated by the centre of mass being slightly shifted to the right. In the intermediate region, the cell tracks appeared oriented in all directions almost equally. In the stiff region, PC-9 cells exhibited a strong tendency to migrate towards softer areas. These observations suggest that PC-9 cells may switch between different migration modes, although further validation is needed. Regarding migration distances, PC-9 cells exhibited extremely low motility with short migration distances as well. In the intermediate and stiff regions, the cells demonstrated markedly higher motility and migrated over longer distances.

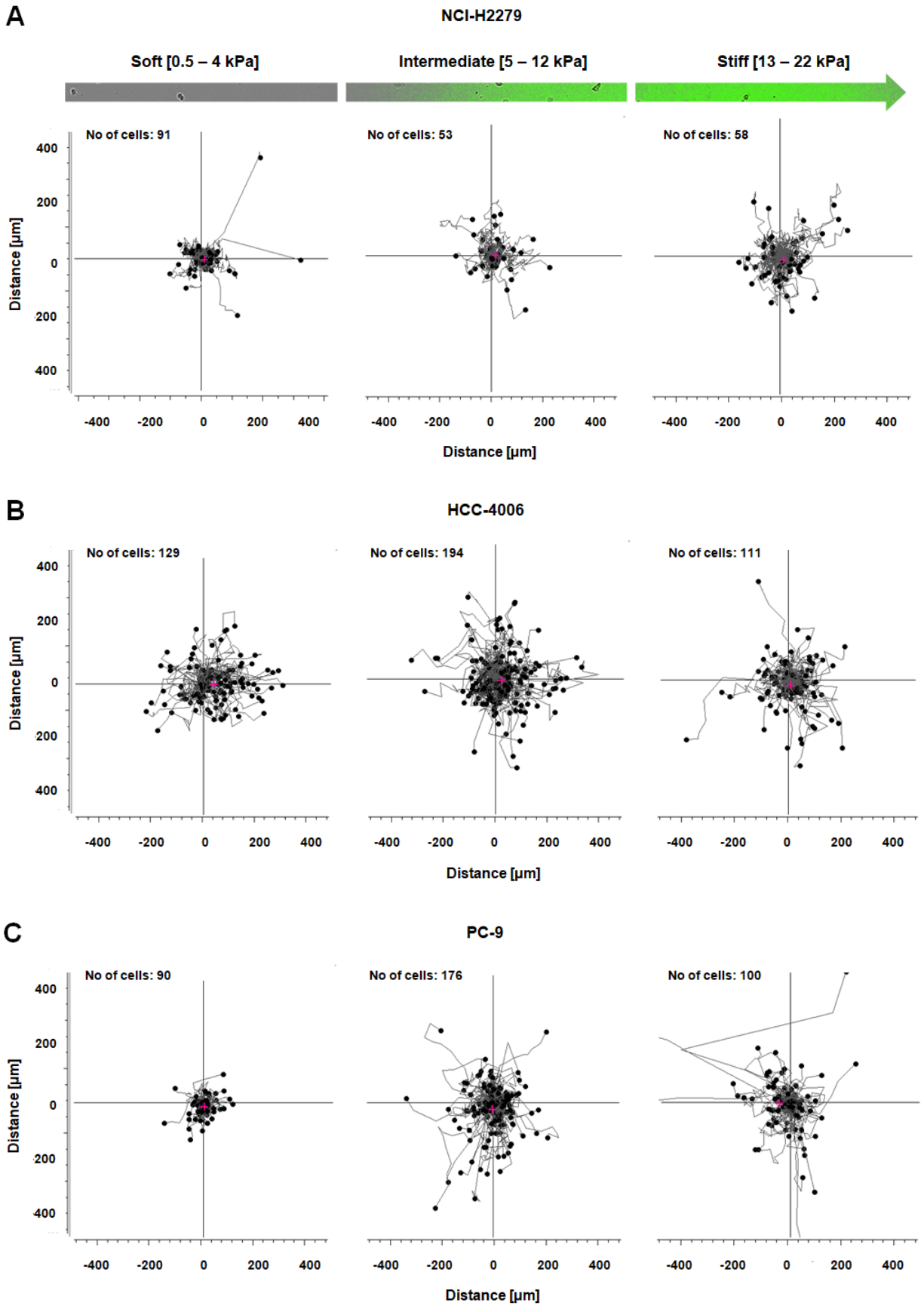

Figure 12. *A-C) Trajectory plots of NCI-H2279 (A), HCC-4006 (*B*), and PC-9 (C) cells seeded on 0.5-22 kPa stiffness gradient. Tracks from individual cells are shown on the soft (left), intermediate (centre), stiff (right) regions. The centre of*

mass is highlighted by a pink (+). A) n = 53–91 cells from two independent experiments. B) n = 111–194 cells from three independent experiments. C) n = 90–176 cells from two independent experiments.

4.3. Lung Cancer Cells Exhibit Differential Responses to Substrate Stiffness

4.3.1. Local Stiffness Influences Durotaxis for HCC-827 and HCC-4006 Cells

To gain a deeper understanding of how matrix stiffness influences the migration of lung adenocarcinoma cells in the aforementioned live-cell imaging - accompanied by single-cell tracking - experiments, we also analyzed two measures of directional migration: angular displacement and the forward migration index (FMI). Angular displacements, referring to the change in direction of each tracked cell over time, were visualized using rose plots to display the distribution of migration directions over time. To assess whether these angular displacement data exhibited significant clustering around a particular direction or were uniformly distributed, we employed the Rayleigh test.

HCC-827 cells exhibited a strong tendency to migrate towards stiffer areas. In the soft region of the gradient, spanning from 0.5 to 4 kPa, the sectors of the rose plot facing the right side of the gradient (the stiffer area) were significantly larger than those facing the opposite direction (***Figure 13A, left panel***). The Rayleigh test yielded a p-value of 0.001, indicating significant direction towards the stiffer area. In the intermediate stiffness range (5 to 12 kPa), these cells continued to migrate towards stiffer areas, as evidenced by the longer sectors of the rose plot oriented towards the stiffer regions and a p-value of 0.014 (***Figure 13A, middle panel***). However, in this stiffness range, the cells moved more laterally and less persistently compared to their movement in the soft region, as the long sectors oriented towards the stiffer area were distributed across various angles. In the stiff region, HCC-827 cells appeared to undergo random migration, with the rose plot sectors distributed almost equally in all directions and a p-value of 0.171 (***Figure 13A, right panel***).

To further quantify the directional bias or persistence of cell migration relative to the stiffness gradient, we calculated the FMI. Specifically, we compared xFMI (displacement of cells along the gradient direction) with yFMI (displacement in directions perpendicular to the gradient). In the soft range of the gradient, xFMI was significantly higher than yFMI, with a p-value of 0.002, indicating a strong directional bias (***Figure 13B, left panel***). However, in the intermediate and stiff regions, xFMI and yFMI values were almost equal, despite significant directionality towards stiffer areas observed in the angular displacement rose plots (***Figure 13B, middle and right panel***).

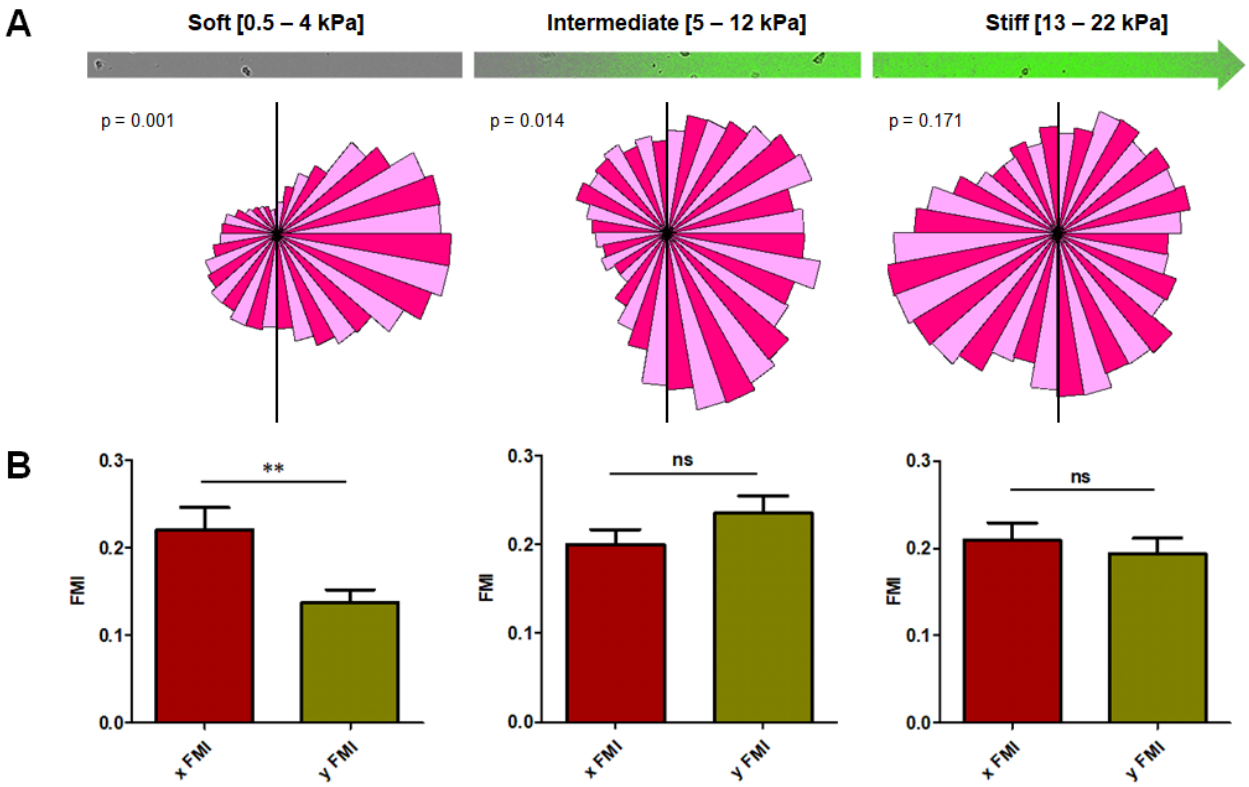

Figure 13. *A) Rose plots representing the angular displacements of individual HCC-827 cells migrating in the soft (left), intermediate (centre) and stiff (right) regions of a 0.5–22 kPa gradient. n = 99–116 cells from three independent experiments. Analyzed by Rayleigh test. C) FMI for cells moving parallel (x FMI) versus perpendicular (y FMI) to the stiffness gradient on the soft, intermediate, or stiff regions. Error bars represent mean ± standard error (SE). n = 99–116 cells from three independent experiments. Analyzed by Wilcoxon signed rank test (∗∗∗p ≤ 0.001, ∗∗p ≤ 0.01, ∗p ≤ 0.05, ns = non significant).*

For further validation of the above findings, we seeded HCC-827 cells on the stiffness gradient gels and quantified the distribution of the cells across the gradient at the start (0 hours) and at the end (24 hours) of the experiment. The cells were fixed at 0 and 24 hours and subsequently stained for nuclei. Fluorescent beads in the gel and cell nuclei were imaged with Nikon AX-R camera, 20x objective lens and we acquired tile scans of the 4 mm x 4 mm middle part of the gel, where the stiffness gradient exists, to visualize the nuclei across the gradient of fluorescent beads. At the beginning of the experiment (0 hours), an even distribution of cells was confirmed (***Figure 16A***). Hexbin plots were created to display the number of cells across the stiffness gradient, providing a visual representation of cell migration after 24 hours.

The tile scans were processed and divided into three vertical sections corresponding to the three stiffness zones: soft (0.5-4 kPa), intermediate (5-12 kPa), and stiff (13-22 kPa). Each section was further divided into four horizontal regions, resulting in 12 smaller regions, each with an area of 1.33 mm^2.

HCC-827 cells appeared to cluster predominantly in the intermediate zone, while fewer cells were observed in the soft and stiff regions. Cell density in each region was calculated by dividing the number of stained nuclei by the area of the region (***Figure 16B***). Our analysis revealed that cell density in the intermediate zone was

almost three times higher than in the soft and stiff zones. There was no significant difference in cell density between the soft and stiff zones.

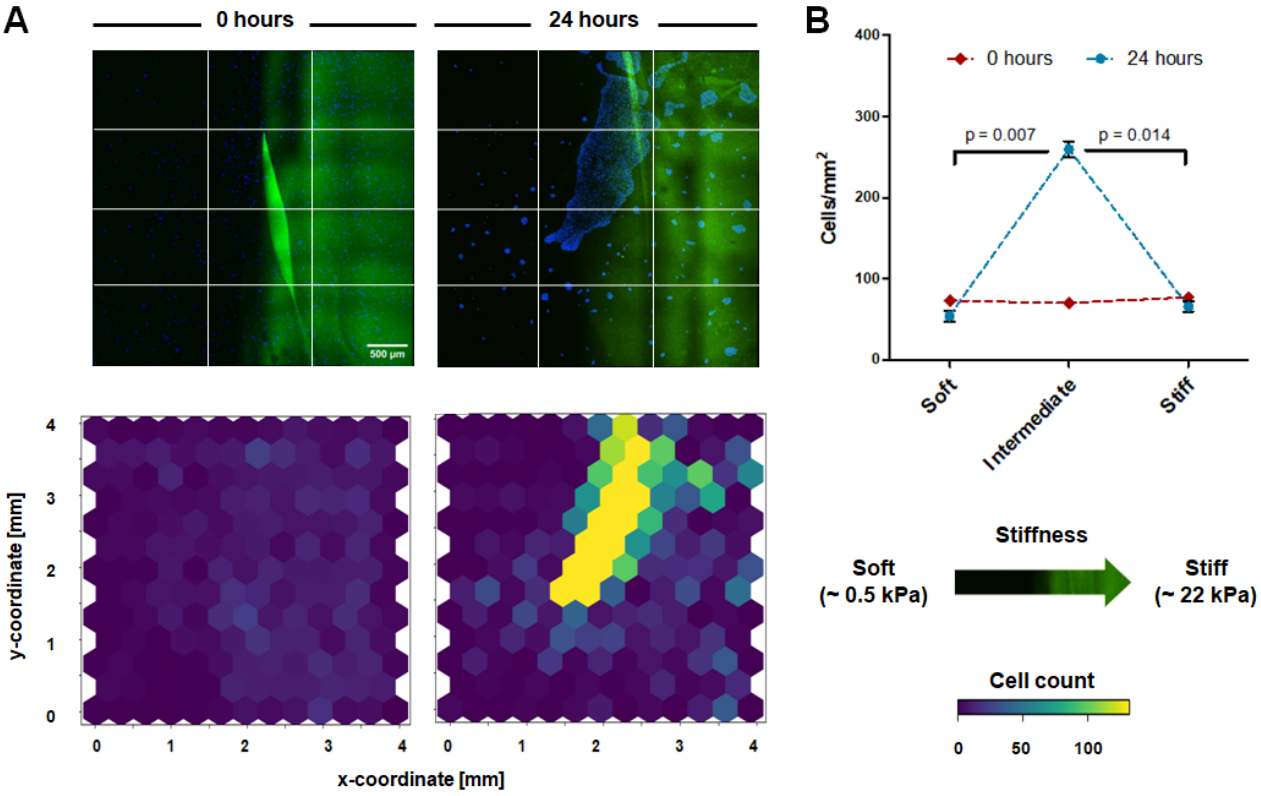

Figure 14. *A) (Top) Representative region of a diffusion-based polyacrylamide stiffness gradient (Young's modulus ~0.5–22 kPa), at the outset of the experiment 24 hours later. HCC-827 cells are indicated by Hoechst nuclear staining. Scale bar, 500 µm. (Bottom) Quantification of cells across the gradient. B) Cell density in different parts of the stiffness gradient. Mean ± SEM of n = 24 ROIs, analyzed by Kruskal-Wallis one-way ANOVA and Dunn's* post hoc *test.*

HCC-4006 cells also displayed a strong tendency to migrate towards stiffer areas, as indicated by the long sectors of the rose plot oriented towards the right side of the gradient in the 0.5–4 kPa stiffness range, with a p-value of 0.0001 (***Figure 15****Figure 15****A, left panel***). These cells continued to exhibit directed migration towards stiffer areas in the intermediate and stiff zones with p-values of 0.0003 and 0.007, respectively (***Figure 15****Figure 15****A, middle and right panel***). However, in these two regions, the movement was less persistent, with the sectors facing the right side of the gradient oriented at various angles rather than a specific direction.

Comparing xFMI and yFMI for HCC-4006 cells revealed a similar pattern to that observed in HCC-827 cells. Specifically, xFMI was significantly higher than yFMI in the 0.5-4 kPa stiffness range, with a p-value of 0.003 (***Figure 15B****Figure 15****, left panel***). In contrast, xFMI and yFMI values were almost equal in the 5-12 kPa and 13-22 kPa stiffness zones (***Figure 15****Figure 15****B, middle and right panel***).

These observations demonstrate that both HCC-827 and HCC-4006 cells undergo durotaxis in the 0.5-4 kPa stiffness range, while this ability of directional movement decreases as cells occupy regions with stiffness greater than 4 kPa. This suggests that local stiffness significantly affects the effectiveness of durotaxis.

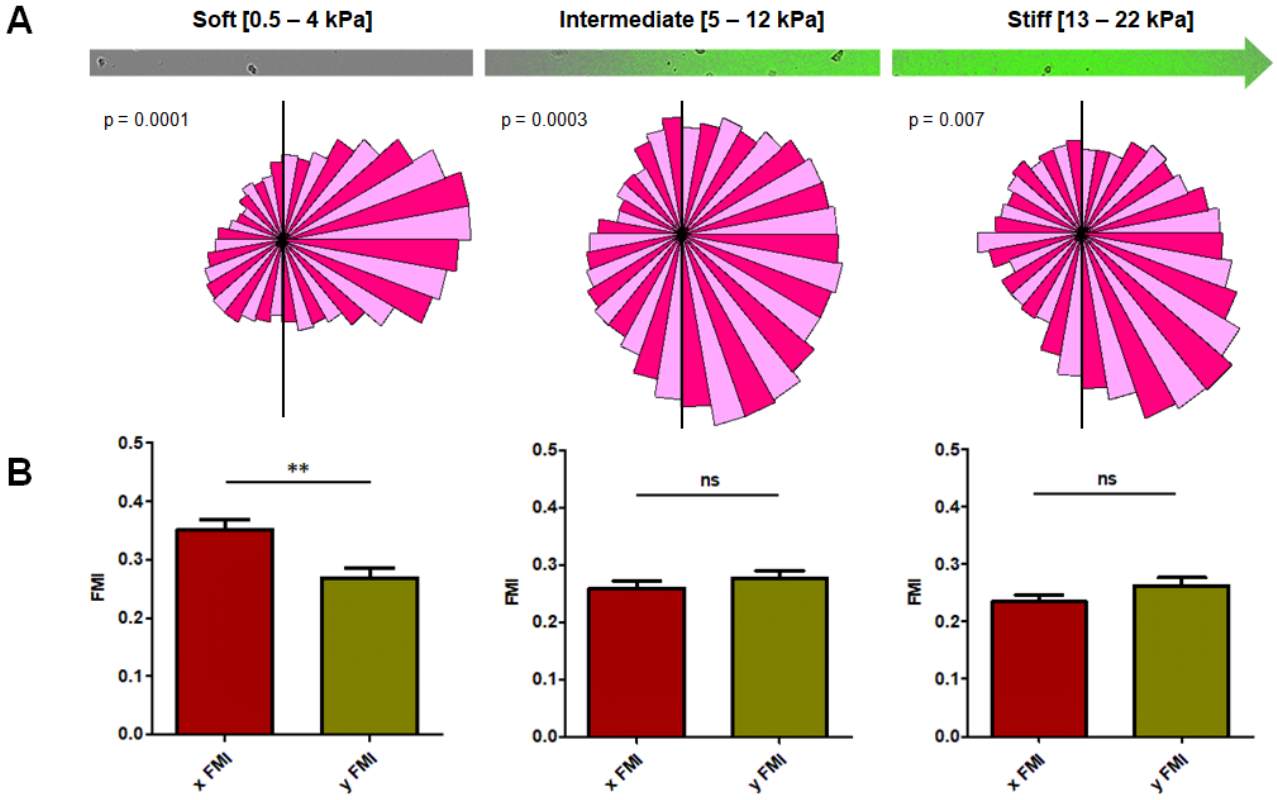

Figure 15. *A) Rose plots representing the angular displacements of individual HCC-4006 cells migrating in the soft (left), intermediate (centre) and stiff (right) regions of a 0.5–22 kPa gradient. n = 111–194 cells from three independent experiments. Analyzed by Rayleigh test. B) FMI for cells moving parallel (x FMI) versus perpendicular (y FMI) to the stiffness gradient on the soft, intermediate, or stiff regions. Error bars represent mean ± standard error (SE). n = 111–194 cells from three independent experiments. Analyzed by Wilcoxon signed rank test (∗∗∗p ≤ 0.001, ∗∗p ≤ 0.01, ∗p ≤ 0.05, ns = non significant).*

4.3.2. NCI-H2279 and PC-9 Cells are Adurotactic

In contrast to the previous findings on HCC-827 and HCC-4006 cell lines, NCI-H2279 cells seem to be adurotactic, exhibiting no directed migration in response to stiffness gradients. Rose plots for NCI-H2279 displayed sectors oriented almost equally in all directions, and the angular displacement data yielded insignificant p-values of 0.065, 0.434, and 0.088 in the soft, intermediate, and stiff zones, respectively, indicating random movement (***Figure 16A***). Additionally, comparisons of xFMI and yFMI values showed insignificant differences, with p-values of 0.281, 0.837, and 0.981 in the soft, intermediate, and stiff regions, respectively (***Figure 16B***).

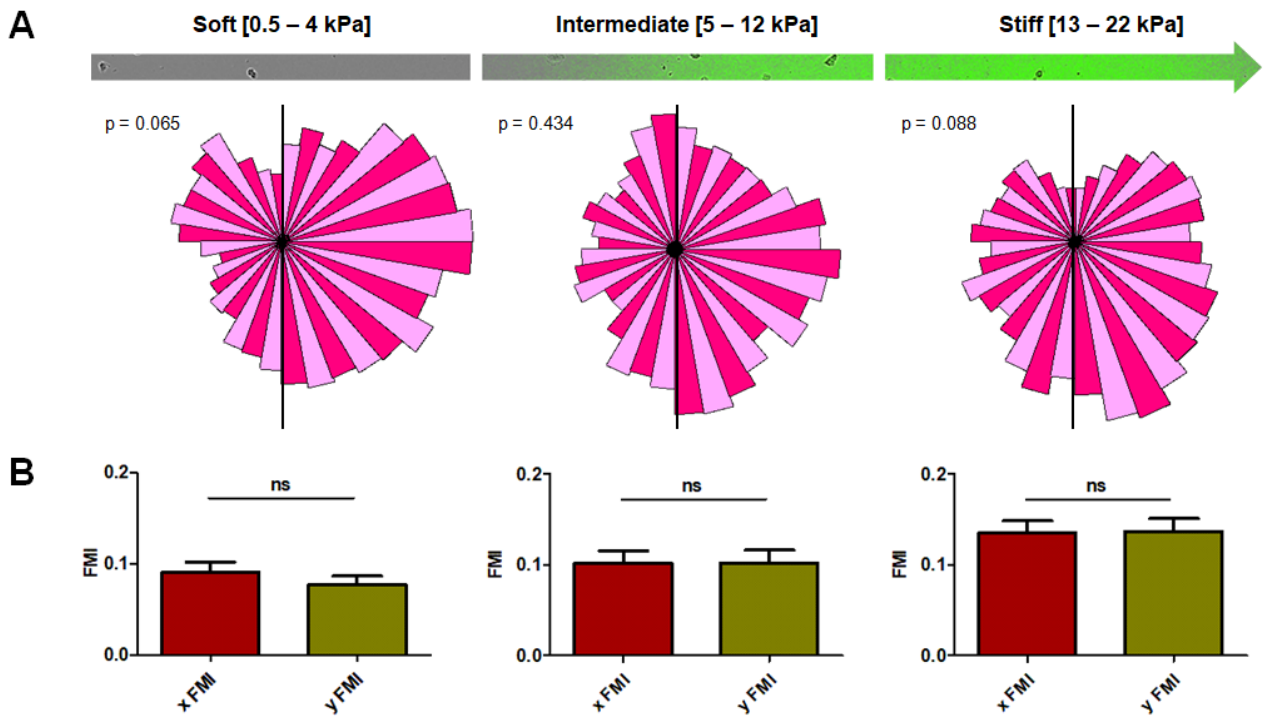

Figure 16. *A) Rose plots representing the angular displacements of individual HCC-2279 cells migrating in the soft (left), intermediate (centre) and stiff (right) regions of a 0.5–22 kPa gradient. n = 43–91 cells from two independent experiments. Analyzed by Rayleigh test. B) FMI for cells moving parallel (x FMI) versus perpendicular (y FMI) to the stiffness gradient on the soft, intermediate, or stiff regions. Error bars represent mean ± standard error (SE). n = 43–91 cells from two independent experiments. Analyzed by Wilcoxon signed rank test (ns = non significant).*

PC-9 cells displayed distinct migratory behaviours across the stiffness gradient gel. In the 0.5-4 kPa range, the rose plot of angular displacement indicated a significant directional migration towards the stiffer region, with some long sectors oriented in that direction at various angles and a p-value of 0.036 (***Figure 17****Figure 17****A, left panel***). Within the intermediate range of 5-12 kPa, these cells exhibited random movement in all directions with a p-value of 0.778 (***Figure 17****Figure 17****A, centre panel***). However, in the stiff region (13-22 kPa), PC-9 cells demonstrated a moderate inclination to migrate towards softer areas, with a p-value of 0.018 (***Figure 17****Figure 17****A, right panel***). Despite this tendency, the rose plot sectors were oriented at various angles, indicating no single preferred direction.

The xFMI and yFMI values were nearly equal for all three stiffness ranges (***Figure 17B***). This was observed despite the rose plot in the soft region indicating a tendency towards durotaxis and the rose plot in the stiff region indicating a tendency towards negative durotaxis.

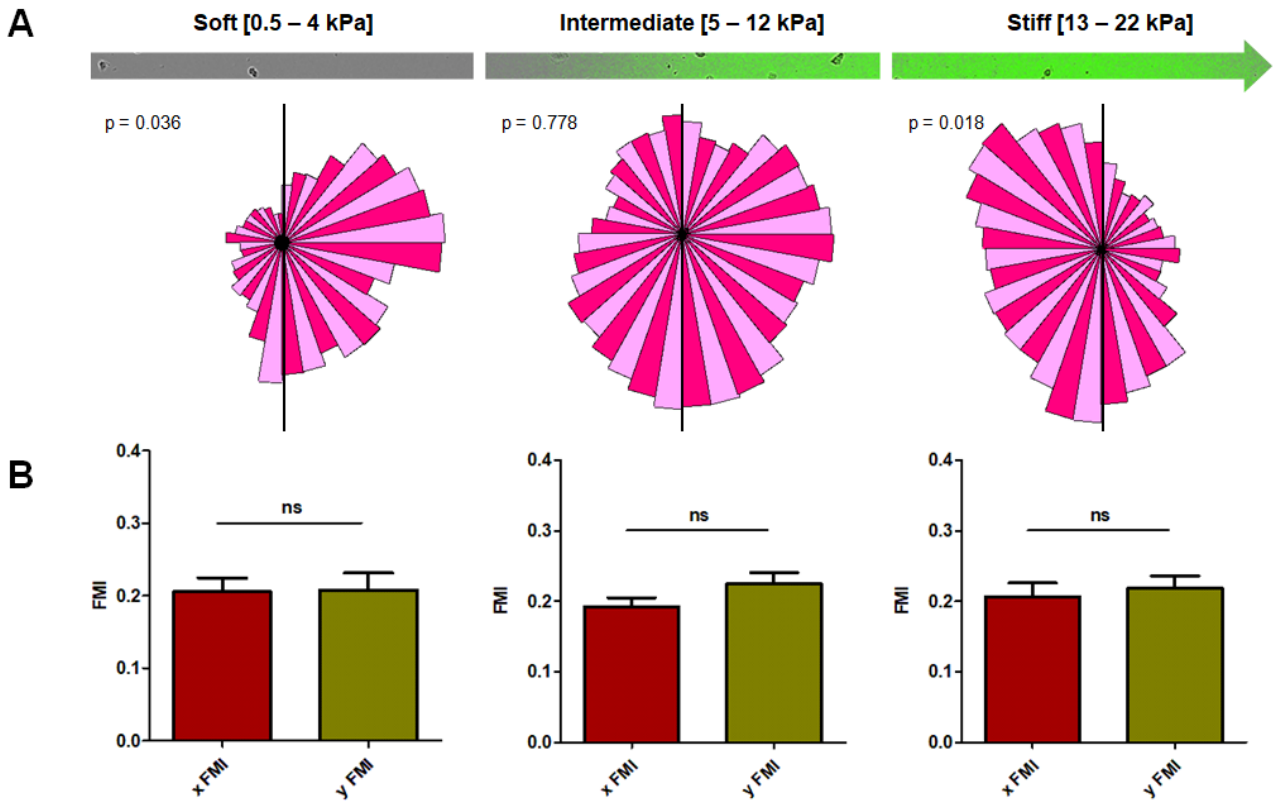

Figure 17. *A) Rose plots representing the angular displacements of individual PC-9 cells migrating in the soft (left), intermediate (centre) and stiff (right) regions of a 0.5–22 kPa gradient. n = 90–176 cells from three independent experiments. Analyzed by Rayleigh test. B) FMI for cells moving parallel (x FMI) versus perpendicular (y FMI) to the stiffness gradient on the soft, intermediate, or stiff regions. Error bars represent mean ± standard error (SE). n = 90–176 cells from three independent experiments. Analyzed by Wilcoxon signed rank test (ns = non significant).*

To further investigate the migratory behaviour of PC-9 cells, we measured cell density across the stiffness gradient over time. The cells were fixed at 0 and 24 hours and subsequently stained for nuclei. 4 mm x 4 mm tile scans of the bead gradient were acquired to visualize nuclei distribution across the fluorescent bead gradient.

Hexbin plots were generated to display the number of cells across the stiffness gradient, providing a visual representation of cell migration after 24 hours. We observed an even distribution of cells at the beginning of the experiment (0 hours) and after 24 hours (***Figure 18A***).

Cell density in each region was calculated by dividing the number of stained nuclei by the area of the region. After 24 hours, the cell density was found to be approximately the same across the entire stiffness gradient, with no significant differences observed between the soft, intermediate, and stiff zones, indicating random movement (***Figure 18B***).

These results suggest that while PC-9 cells may exhibit some directional preferences based on substrate stiffness, their overall migratory behaviour seems random, complex and variable across different stiffness environments.

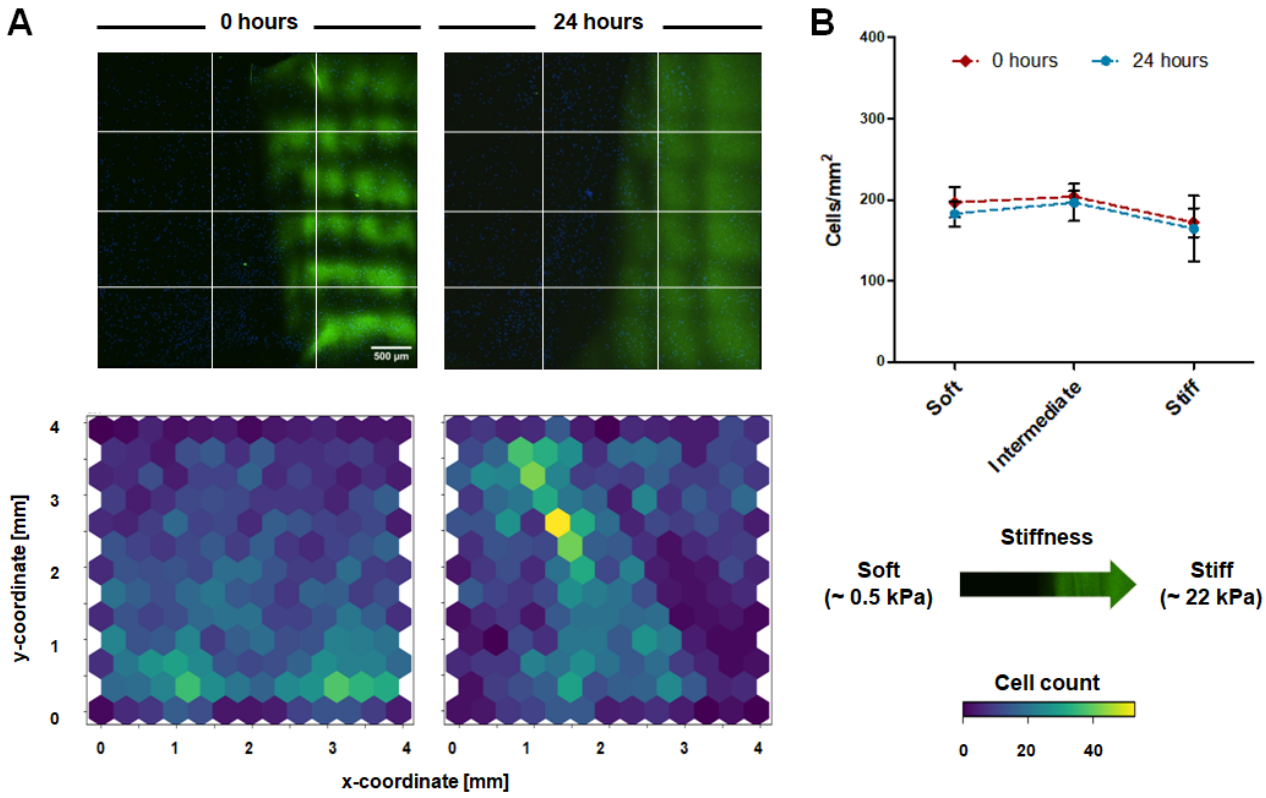

Figure 18. *A) (Top) Representative region of a diffusion-based polyacrylamide stiffness gradient (Young's modulus ~0.5–22 kPa), at the outset of the experiment 24 hours later. PC-9 cells are indicated by Hoechst nuclear staining. Scale bar, 500 µm. (Bottom) Quantification of cells across the gradient. B) Cell density in different parts of the stiffness gradient. Mean ± SEM of n = 12 ROIs, analyzed by Kruskal-Wallis one-way ANOVA and Dunn's* post hoc *test.*

4.4. Influence of Substrate Stiffness on Cell Migration Speed

To further elucidate the relationship between cell movement characteristics and substrate stiffness, we measured cell speed across different stiffness gradients. Our results indicate that HCC-827 cells exhibit significantly slower movement in the soft region (0.5-4 kPa), where they display durotactic migration, compared to their movement in the stiffer regions of the gradient. Specifically, HCC-827 cells demonstrated a mean speed of approximately 0.2 μm per minute in the 0.5-4 kPa range, while their mean speed increased to 0.4 μm per minute in the 4-22 kPa range (***Figure 19A***). In contrast, HCC-4006 cells maintained a consistent speed of 0.4 μm per minute across the entire 0.5-22 kPa stiffness range (***Figure 19B***). These findings suggest that higher cell speed does not enhance durotaxis.

Furthermore, we observed that the migration speed of NCI-H2279 and PC-9 cells was also affected by substrate stiffness. Both cell lines exhibited lower speeds in the soft stiffness range and increased their speeds in progressively stiffer regions. Specifically, NCI-H2279 cells moved at approximately 0.4 μm per minute in the 0.5-4 kPa range and increased their speed to about 0.5 μm per minute in the intermediate and stiff regions (***Figure 19C***). PC-9 cells displayed a more pronounced increase in speed, from 0.2 μm per minute in the soft region to 0.4 μm per minute in the intermediate region, and 0.6 μm per minute in the stiff region (***Figure 19D***).

Therefore, even though NCI-H2279 and PC-9 cells are adurotactic, they still exhibit sensitivity to substrate stiffness and adjust their migration speed accordingly. These results indicate that while durotaxis is not directly correlated with higher migration speeds, substrate stiffness nonetheless plays a significant role in modulating cell motility.

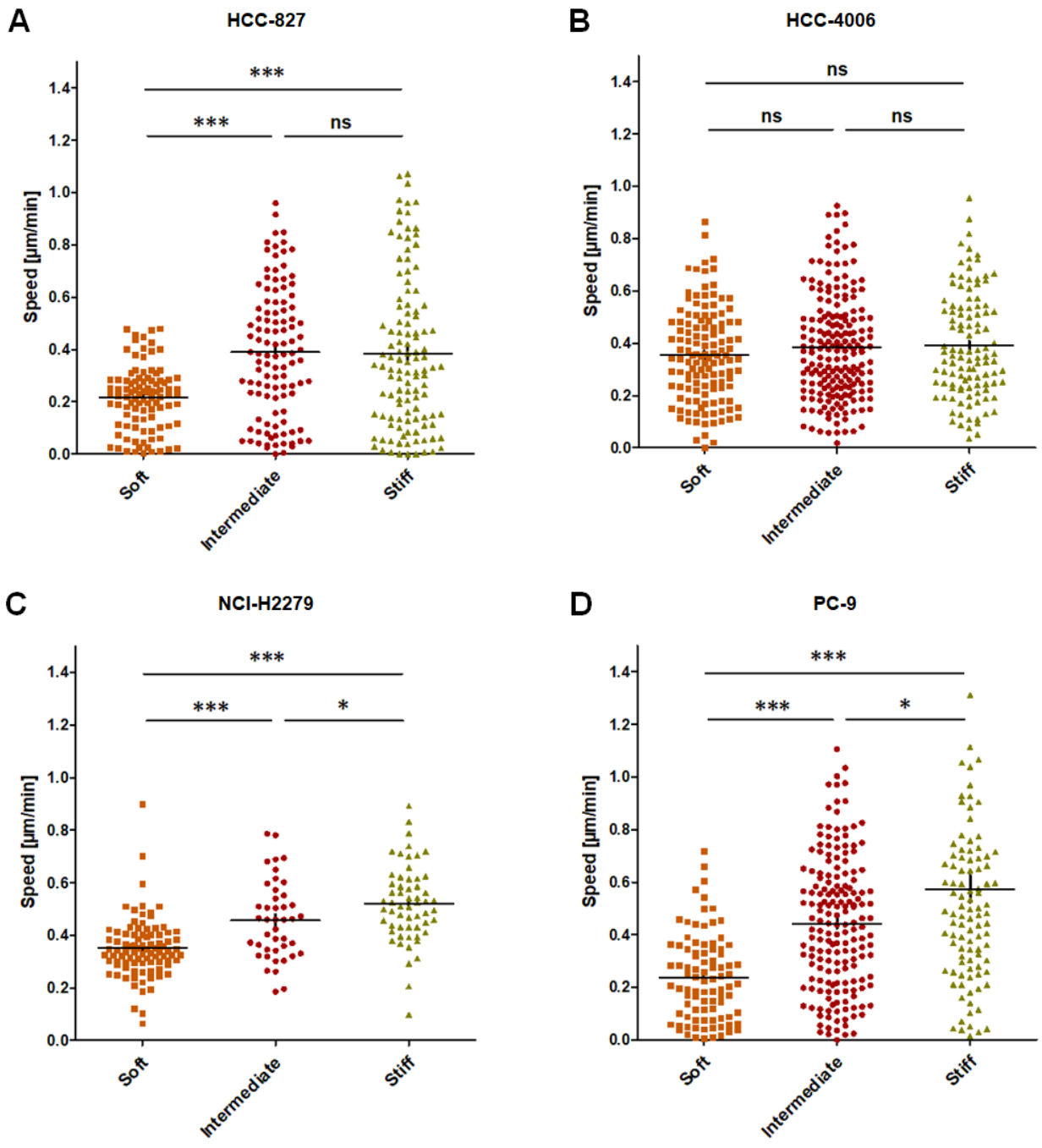

Figure 19. *Speed of A) HCC-827, B) HCC-4006, C) NCI-H2279, and D) PC-9 with respect to position on the gradient. Error bars represent mean ± SE. Evaluated by one-way ANOVA and Tukey's post hoc test (***p ≤ 0.001, **p ≤ 0.01, *p ≤ 0.05, ns = non significant).*

4.5. Influence of Substrate Stiffness on Cell Migration Distance

Measuring the mean distance migrated by cells in response across the stiffness gradient gels revealed significant variations among the four NSCLC cell lines.

HCC-827 cells exhibited a marked difference in migration distance across the stiffness gradient. In the soft stiffness range (0.5-4 kPa), these cells had a mean migration distance of 100 μm. As the stiffness increased to the intermediate range (5-12 kPa), their migration distance doubled to 200 μm. Interestingly, this enhanced migratory response reached a plateau in the stiffest region (13-22 kPa), maintaining the same 200 μm distance. This pattern suggests that HCC-827 cells respond to increasing stiffness by enhancing their migration distance up to intermediate stiffness levels, beyond which their migration does not further increase despite higher stiffness.

Conversely, HCC-4006 cells maintained a consistent migration distance of approximately 200 μm across the entire stiffness gradient.

NCI-H2279 and PC-9 cell lines demonstrated a significant increase in migration distance in response to stiffer substrates. NCI-H2279 cells migrated an average distance of 250 μm in the 0.5-4 kPa range. This distance increased to nearly 350 μm in the intermediate range (5-12 kPa) and further to 400 μm in the stiffest region (13-22 kPa). Similarly, PC-9 cells showed a progressive increase in migration distance: 100 μm in the soft region, 200 μm in the intermediate range, and almost 300 μm in the stiffest region.

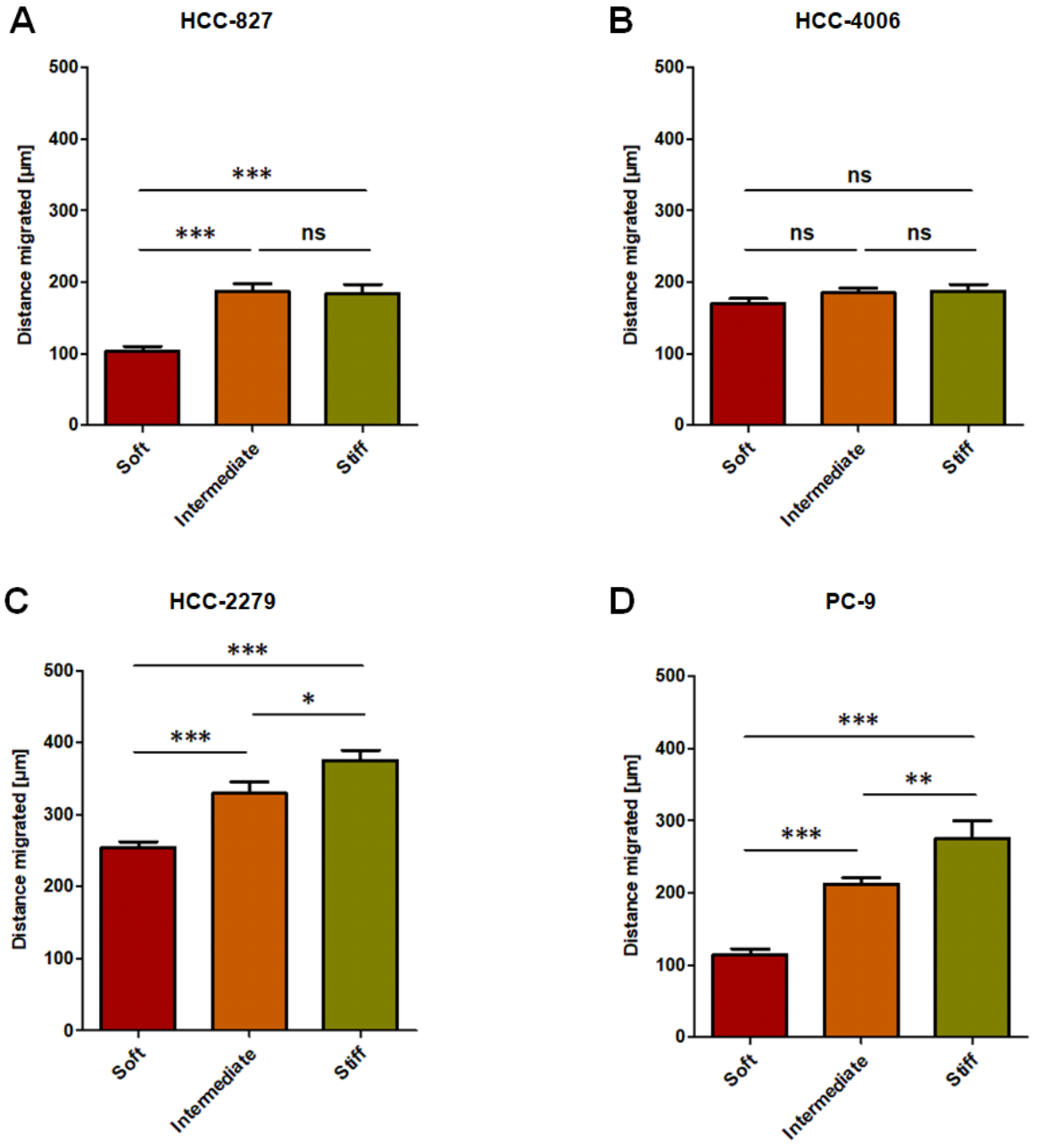

Figure 20. *Distance migrated by A) HCC-827, B) HCC-4006, C) NCI-H2279, and D) PC-9 with respect to position on the gradient. Error bars represent mean ± SE. Evaluated by one-way ANOVA and Tukey's post hoc test (∗∗∗p ≤ 0.001, ∗∗p ≤ 0.01, ∗p ≤ 0.05, ns = non significant).*

4.6. Actin Cytoskeleton Phenotype Variability in Response to Stiffness Gradient

Numerous studies on normal cells, including fibroblasts, smooth muscle cells, and neural cells, have demonstrated that substrate stiffness significantly influences the morphology of the actin cytoskeleton, which in turn affects cell shape and promotes a larger spreading area on stiffer substrates (Engler, Richert, Wong, Picart, & Discher, 2004; Gu et al., 2012; Pelham Jr & Wang, 1997). Cells typically exhibit increased spreading and contractility on stiff matrices, resulting in a larger cell area. In contrast, soft substrates tend to result in a less developed cytoskeleton, more circular cell shapes, and reduced cell spreading (Jay D. Humphrey, Eric R. Dufresne, & Martin A. Schwartz, 2014; Peyton & Putnam, 2005).

We hypothesized that lung cancer cells might similarly exhibit changes in the actin cytoskeleton when exposed to a stiffness gradient. To test this, we cultured HCC-827 and PC-9 cells on the stiffness gradient gels. After 24 hours, the cells were stained for actin. Focusing on the 0.5-6 kPa range, where HCC-827 cells undergo durotaxis, we measured cell area and circularity of single cells and calculated the underlying stiffness value for each cell according to the method described in section *3.7.1. Stiffness Characterization*.

Our observations revealed that both cell lines displayed highly heterogeneous actin phenotypes across the gradient. Consequently, no correlation was found between the actin cytoskeleton and substrate stiffness.

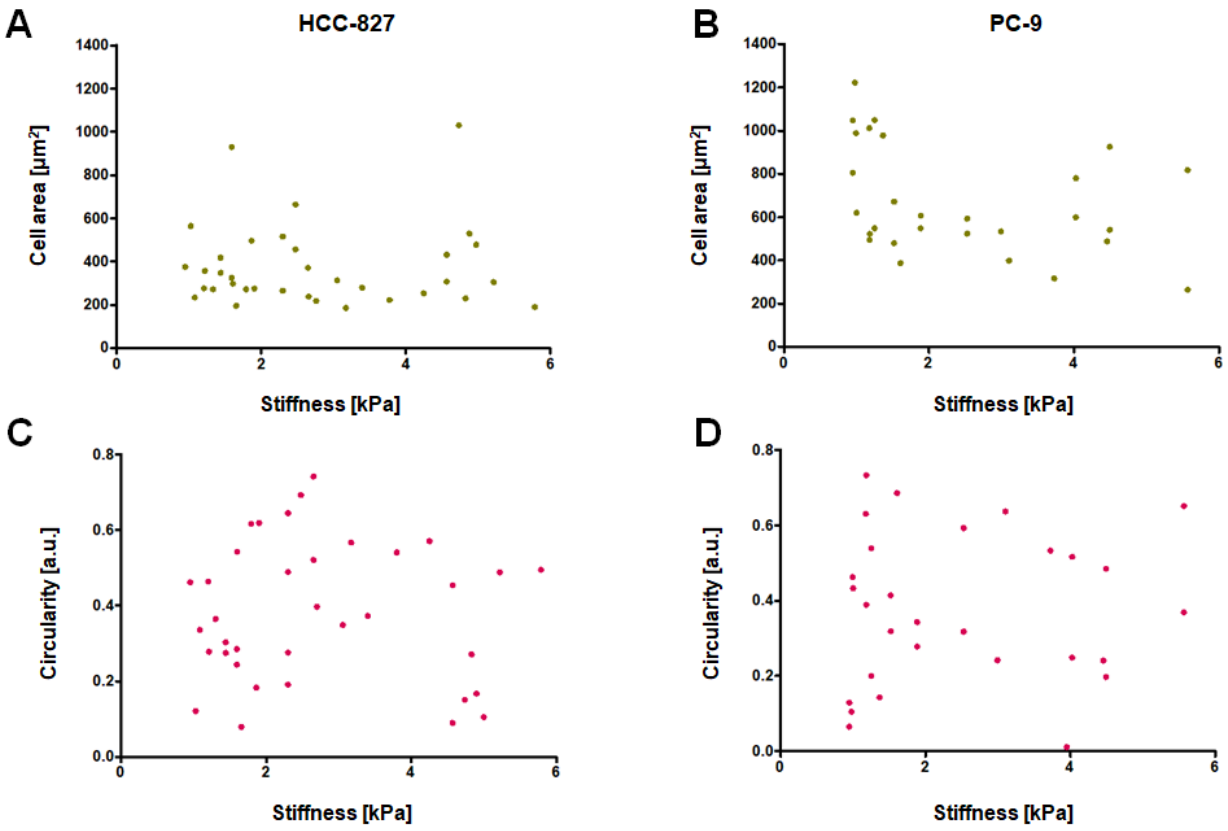

Figure 21. *Actin cytoskeleton across the 0.5-6 kPa stiffness gradient. A) Cell area [µm²] of HCC-827 cells n=36 cells from two independent experiments. B) Cell area [µm²] of PC-9 cells n=36 cells from two independent experiments. C) Circularity [a.u.] of HCC-827 cells n=29 cells from two independent experiments. D) Circularity [a.u.] of PC-9 cells. n=29 cells from two independent experiments.*

5. Discussion

Tumourigenesis is driven by two main factors: genetic and epigenetic alterations within tumour cells, and the dynamic interactions within the tumour microenvironment. The tumour microenvironment, known for its immunosuppressive properties, consists of blood vessels, immune cells, stromal cells, and the extracellular matrix. The ECM, primarily composed of proteins, such as fibrous proteins and glycosaminoglycans, delivers vital biochemical and mechanical cues to resident cells, thereby maintaining tissue homeostasis.

Matrix stiffness, defined as the ECM's resistance to deformation under mechanical stress, is a critical mechanical property of tissues. This property is quantitatively measured by the elastic modulus. Under physiological conditions, ECM rigidity is precisely regulated, playing an essential role in controlling various cellular processes such as proliferation, differentiation, and migration, while also maintaining tissue architecture. Aberrant alterations in ECM stiffness are implicated in numerous pathological conditions, particularly cancer. Increased tissue matrix stiffness is a hallmark of many solid tumours. For instance, the stiffness of solid lung cancers (20–30 kPa) markedly exceeds that of normal lung parenchyma (0.5–5 kPa) (Miyazawa et al., 2018). Key regulators of ECM remodelling in cancer include the activation of cancer-associated fibroblasts and the accumulation and altered cross-linking of ECM proteins, such as collagen, which contribute to increased stiffness.

Durotaxis, the directed migration of cells towards stiffer areas of the ECM, has been well-characterized in several non-malignant cell types. However, research into whether cancer cells can also exhibit effective durotaxis has been limited. Specifically, durotaxis has been reported only in four cell lines: U87-MG and T98G glioblastoma cells, MDA-MB-231 metastatic epithelial breast cancer cells, and HT1080 fibrosarcoma cells (DuChez et al., 2019). Recent studies have shown that U-251MG glioblastoma cells and B16 F1 and F10 acral melanoma cells exhibit negative durotaxis, a form of directed cell migration towards softer environments (Huang et al., 2022; Aleksi Isomursu et al., 2022). Additionally, adurotactic migration, characterized by a lack of directed migration in response to matrix stiffness, has been observed in PC-3 metastatic prostate cancer cells and NCI-H1299 metastatic lung adenocarcinoma cells (Yeoman et al., 2021).

Understanding how extracellular matrix stiffness influences cancer cell migration is crucial for advancing our knowledge of tumour progression and metastasis. Evidence indicates that tumour matrix stiffness is significantly elevated compared to normal tissues and correlates strongly with disease progression, metastasis, and clinical outcomes across several cancer types, including breast cancer, colorectal cancer, hepatocellular carcinoma, and pancreatic ductal adenocarcinoma (Kalli & Stylianopoulos, 2018; Reid et al., 2017). Studies using atomic force microscopy (AFM) on breast tumour mastectomies have shown that the invasive front of tumours tends to be stiffer than the cancerous mass itself (Acerbi et al., 2015). This gradient in stiffness may provide an opportunity for cancer cells to escape from harsh conditions like hypoxia and necrosis at the primary site. Notably, migrating towards areas of higher stiffness not only aids in the escape of cancer cells but also enhances their ability to effectively proliferate and promotes tumour growth, as supported by various studies (Bae et al., 2014; Schrader et al., 2011; Umesh et al., 2014). Interestingly though, in advanced stage lung cancer in which intrapulmonary metastases often occur, the metastatic cells need to migrate from a stiffer area (the primary tumour) towards a softer area of the lung.

In this thesis, we utilized an established protocol for generating polyacrylamide hydrogels with a continuous stiffness gradient ranging from 0.5 to 22 kPa (Barber-Pérez et al., 2020). The current hydrogels can be easily and quickly fabricated in any laboratory without the need of specific equipment and at low-cost. Moreover, they are circular, with a diameter of 14 mm and a thickness of approximately 80 ± 100 μm, facilitating high-resolution imaging. A notable aspect of this method is the incorporation of fluorescent beads into the hydrogels, where bead density positively correlates with gel stiffness. This allows for the quantification of stiffness across the gradient without the need for AFM, using a bead density and stiffness correlation equation.

Our observations revealed that these hydrogels comprise two large uniform stiffness regions on its left and right sides, with values of 0.5 kPa and 22 kPa, respectively. Between these regions lies a smaller central area, approximately 2-4 mm wide, where the bead gradient is present. Consequently, the gradient region occupies a relatively small portion of the total gel area. This limitation arises from the technique used to establish the stiffness gradient. The covering of adjacent drops with a coverslip restricts diffusion to a limited distance, thus only cells positioned within this small central region can yield insights into the mechanoresponse to the stiffness gradient. Within this 4 mm wide central region, where the stiffness gradient spans, we identified three distinct stiffness zones:

- **Soft zone (~0.5-4 kPa):** This region, located on the left side of the hydrogel, has either no beads or a very low quantity of beads.
- **Intermediate zone (~5-12 kPa):** This region, situated in the middle part of the gel, exhibits a gradient of mild to intense fluorescence.
- **Stiff zone (~13-22 kPa):** This region, found on the right side of the gel, has the highest bead fluorescence.

These stiffness values were consistent across all hydrogels, with only minor variations of 0.5 to 1 kPa.

Another drawback of this technique is the slight tilt of the hydrogel surface towards its softer region, causing variations in height levels that may introduce additional mechanical-geometric cues beyond stiffness. Addressing this issue is crucial, as it can potentially confound experimental outcomes. While this challenge persists, minimizing its impact can be achieved by ensuring the workbench surface is perfectly horizontal during fabrication.

Furthermore, a significant issue with this methodology arises during the removal of the coverslip after polyacrylamide polymerization. This delicate process requires the use of medical tweezers and a bent needle, demanding careful handling to prevent coverslip breakage and the formation of small wrinkles on the gel surface. Another concern is the tendency of the polyacrylamide to adhere to the coverslip, which can result in unintentional tearing of the gel when attempting to detach the coverslip. To mitigate these problems, pre-treating the coverslips with chlorosilane to impart hydrophobic properties facilitates easier removal when adding PBS.

The **first aim** of this thesis was to evaluate the response of lung cancer cells to substrate stiffness, particularly their potential to exhibit durotaxis. Both HCC-827 and HCC-4006 cell lines displayed a pronounced tendency

to migrate towards stiffer regions in the soft zone (~0.5-4 kPa). This was evident from both the angular displacement data and the comparison between xFMI and yFMI values. Unexpectedly, in the intermediate and stiff regions, the xFMI and yFMI values were almost equal for both cell lines, despite significant directionality towards stiffer areas observed in the angular displacement rose plots. This suggests that these cells exhibit durotaxis primarily in softer environments, but their directed movement diminishes in stiffer conditions.

The ability of both cell lines to undergo durotaxis appears to depend significantly on the local compliance of the stiffness gradients, with maximal durotaxis observed in the soft 0.5-4 kPa range. In the 5-22 kPa range, HCC-827 and HCC-4006 continued to move towards the stiffer regions, as indicated by the angular displacement data. However, xFMI and yFMI values being almost equal suggest low directionality of movement. This finding aligns with previous research indicating that there is a plateau or saturation in the efficiency of durotaxis above an optimal range of stiffness, although durotaxis can still occur in regions of high stiffness (DuChez et al., 2019). Specifically, four cancer cell lines exhibited durotaxis on a stiffness gradient ranging from 2 to 7 kPa, whereas their ability to undergo durotaxis was limited on higher stiffness levels.

Overall, these observations suggest the involvement of other biochemical paracrine signals. At higher stiffness levels, the mechanical cue of substrate stiffness may weaken, allowing biochemical cues to dominate. As previously observed for chemotactic gradients, high levels of a chemoattractant can inhibit chemotaxis due to receptor saturation (Tweedy, Knecht, Mackay, & Insall, 2016). Thus, both chemo- and duro-taxis may require optimal concentrations of the respective chemical or physical signals, in order to be efficient.

Considering the potential biological significance of durotaxis in human cancer cells, it is essential to recognize that malignant cells often navigate a multifaceted microenvironment. This environment provides both chemical and mechanical cues that regulate cell adhesion and migration. This interplay between mechanical and biochemical signals in directing cell movement could result in a combined effect of chemo- and duro-taxis. Understanding this balance between mechanical and biochemical signals is crucial, as it highlights the complexity of cellular responses to their environment.

Moreover, hexbin plots showing the cell density across the gel at 0 and 24 hours revealed that HCC-827 cells clustered more at an intermediate stiffness. This suggests that they may have undergone durotaxis up to that stiffness level, but in stiffer regions, durotaxis wasn't efficient enough for cells to travel to the 13-22 kPa range. However, these observations might be attributed to varying levels of proliferative capacity when these cells are seeded on different stiffness levels. It is known that cancer cells proliferate and form clusters to generate tumours (J. Lee et al., 2015; Nukuda et al., 2015; Yuan, Zhong, Ma, Zhang, & Tian, 2015). Specifically, a stiff matrix enhances the proliferative ability of NSCLC NCI-H460SM, A549 and SPCA-1 cell lines (Navab et al., 2016; Yuan et al., 2015).

Additionally, the efficiency of durotaxis may be influenced by technical parameters, such as the ECM component used as the coating protein for the gels. Different ECM proteins, including collagen I, fibronectin, and laminin, bind to distinct integrins and can trigger different intracellular signalling pathways that affect cell migration. For example, vascular smooth muscle cells display durotaxis on gradients coated with fibronectin,

but not laminin (C. D. Hartman, B. C. Isenberg, S. G. Chua, & J. Y. Wong, 2016). We chose collagen I for our PA hydrogels because it is the most abundant protein in the lung ECM, aiming to mimic the lung's native tissue environment. However, other studies investigating durotaxis in various cancer cell lines tend to use fibronectin as the coating protein (DuChez et al., 2019; Huang et al., 2022; A. Isomursu et al., 2022), which may yield different results.

NCI-H2279 cell line exhibited adurotactic behaviour, displaying random movement across all stiffness zones. However, these cells still seem to sense and respond to matrix stiffness, as evidenced by the varying lengths of the tracks in the trajectory plots across the three stiffness range zones. This behaviour might be attributed to the ECM composition, as mentioned above.

PC-9 cells, as illustrated by the angular displacement rose plots, preferred stiffer areas within the 0.5-4 kPa range but moved towards softer areas in the 13-22 kPa zone. In the intermediate 5-12 kPa range, PC-9 cells exhibited random migration in all directions. These observations are consistent with previous research on U-251MG glioblastoma cells cultured on stiffness gradient hydrogels ranging from 0.5-22 kPa. These cells migrated towards an intermediate stiffness level, approximately 10 kPa, demonstrating both positive and negative durotaxis depending on their spatial orientation within the gradient (A. Isomursu et al., 2022). Thus, the transition between these two migration modes enabled glioblastoma cells to attain an optimal stiffness. Despite these migratory tendencies of PC-9 cells, the xFMI and yFMI values did not indicate a clear directional bias. Additionally, the hexbin plots showed uniform cell density across the stiffness gradient gel after 24 hours, suggesting a complex migratory behaviour that that requires further investigation to be fully understood.

These results collectively suggest that substrate stiffness significantly affects the migratory behaviour of lung adenocarcinoma cells, with variations observed among different cell lines. The ability of some cancer cells to migrate towards softer or stiffer environments may have significant implications for cancer progression and metastasis. Further research is needed to elucidate the complex relationship between mechanical and biochemical cues in cancer cell migration, the underlying mechanisms of durotaxis and its variations in different cancer cell types.

The **second aim** of the current thesis was to explore the impact of substrate stiffness on the migratory behaviour and motility of lung cancer cells, examining additional migration parameters such as cell speed and distance migrated.

Our investigation into cell speed and migration distance across different stiffness gradients revealed that HCC-827 cells displayed lower speeds and travelled in shorter distances in the soft region compared to stiffer regions. This contrasts with findings for the BJ-5ta normal fibroblast line, which showed consistent speeds across all stiffness levels despite exhibiting elevated durotaxis in the soft region (DuChez et al., 2019). This suggests that while durotaxis is evident in lower stiffness ranges, higher stiffness may enhance cell motility but not necessarily directed migration. Thus, speed of migration does not affect the efficiency of durotaxis.

For NCI-H2279 and PC-9 cells, increased stiffness correlated with increased migration distances and speeds, despite their adurotactic behaviour. This indicates that substrate stiffness can modulate cell motility

independently of durotaxis, which is consistent with the understanding that mechanical cues in the extracellular matrix can influence various aspects of cell behaviour (Pelham Jr & Wang, 1997; Peyton & Putnam, 2005). Interestingly, adurotactic cancer cells exhibit higher velocity in stiffer environments, which contributes to their metastatic potential (Yeoman et al., 2021).

However, HCC-4006 cells showed the same speed across the gradient. It is important to highlight that this cell line originates from a metastatic site of the tumour, while the other three cell lines (HCC-827, NCI-H2279, and PC-9) are derived from primary tumour sites. The observation that HCC-4006 cells undergo robust durotaxis despite maintaining steady migration metrics across different stiffness levels suggests a nuanced adaptation in their mechanosensitive behaviour compared to primary tumour cell lines. This indicates potentially optimized migration strategies developed during metastatic progression, balancing responsiveness to mechanical cues with other factors crucial for metastatic dissemination, such as chemotaxis. Understanding these distinct responses among cancer cell lines could provide critical insights into the diverse strategies employed by cells during metastatic spread in cancer therapy. To our knowledge, this study is the first to document such differences in the migratory behaviour between primary and metastatic cell lines.

The examination of the actin cytoskeleton in response to substrate stiffness revealed highly heterogeneous phenotypes across the stiffness gradient for both HCC-827 and PC-9 cells. Despite expectations, no clear correlation was found between actin organization and substrate stiffness in lung cancer cells. This heterogeneity could be attributed to the intrinsic variability within cancer cell populations and their ability to adapt to diverse mechanical environments, which may involve complex signalling pathways and cytoskeletal remodelling mechanisms.

6. Conclusions

In this thesis, we have established that lung adenocarcinoma cancer cells exhibit a rich palette of responses to matrix stiffness and added durotaxis as a potential contributor to lung cancer. These observations contribute substantially to the field of cancer cell mechanobiology and could provide additional biological significance to the alterations in stiffness known to exist at tumour sites.

Key findings include:

- HCC-827 and HCC-4006 cell lines undergo durotaxis, i.e., directed cell migration toward regions of increasing stiffness.
- Durotaxis occurred most efficiently on a soft substrate and became less effective on stiffer substrates.
- NCI-H2279 and PC-9 cell lines exhibited adurotactic behaviour, migrating randomly regardless the local stiffness.
- HCC-827, NCI-H2279 and PC-9 cell lines migrate longer distances and at higher speeds as the stiffness levels increase.
- HCC-4006 cell line maintains constant migration distance and speed across the stiffness gradient.
- Actin cytoskeleton morphology is highly heterogeneous among cells across the stiffness gradient.

7. Implications and Future Directions

These findings underscore the complexity of cancer cell migration and the role of substrate stiffness in influencing cancer cell behaviour. The differential responses observed among these four EGFR-driven NSCLC cell lines highlight the importance of considering cell-specific characteristics when studying mechanosensitive behaviours such as durotaxis.

Future research should focus on elucidating the molecular mechanisms underlying these differential responses to substrate stiffness. This includes investigating expression levels of specific integrins that bind collagen and mechanosensitive adhesion proteins such as paxillin, talin, and vinculin. Moreover, assessing the levels of phosphorylation/activation of mechanoregulators such as FAK and myosin II light chain would provide further insights.

Furthermore, exploring the role actin-myosin cytoskeleton could provide vital information about the mechanisms of durotaxis in cancer cells. Experimental approaches involving ROCK and myosin II inhibitors could be employed to assess potential alterations in the migratory patterns of each NSCLC cell line.

Additionally, using alternative ECM components such as fibronectin instead of collagen I as coating proteins of PA hydrogels could offer further insights into how varying ECM compositions influence cancer cell responses to mechanical cues.

References

Acerbi, I., Cassereau, L., Dean, I., Shi, Q., Au, A., Park, C., . . . Weaver, V. (2015). Human breast cancer invasion and aggression correlates with ECM stiffening and immune cell infiltration. *Integrative Biology, 7*(10), 1120-1134.

Affo, S., Yu, L.-X., & Schwabe, R. F. (2017). The role of cancer-associated fibroblasts and fibrosis in liver cancer. *Annual Review of Pathology: Mechanisms of Disease, 12*, 153-186.

Alberts, B. (2017). *Molecular biology of the cell*: Garland science.

Ashrafi, A., Akter, Z., Modareszadeh, P., Modareszadeh, P., Berisha, E., Alemi, P. S., . . . Zhang, L. (2022). Current Landscape of Therapeutic Resistance in Lung Cancer and Promising Strategies to Overcome Resistance. *Cancers (Basel), 14*(19). doi:10.3390/cancers14194562

Bae, Y. H., Mui, K. L., Hsu, B. Y., Liu, S.-L., Cretu, A., Razinia, Z., . . . Assoian, R. K. (2014). A FAK-Cas-Rac-lamellipodin signaling module transduces extracellular matrix stiffness into mechanosensitive cell cycling. *Science signaling, 7*(330), ra57-ra57.

Barber-Pérez, N., Georgiadou, M., Guzmán, C., Isomursu, A., Hamidi, H., & Ivaska, J. (2020). Mechano-responsiveness of fibrillar adhesions on stiffness-gradient gels. *J Cell Sci, 133*(12). doi:10.1242/jcs.242909

Barros, C. S., Franco, S. J., & Müller, U. (2011). Extracellular matrix: functions in the nervous system. *Cold Spring Harbor perspectives in biology, 3*(1), a005108.

Beri, P., Matte, B. F., Fattet, L., Kim, D., Yang, J., & Engler, A. J. (2018). Biomaterials to model and measure epithelial cancers. *Nature Reviews Materials, 3*(11), 418-430. doi:10.1038/s41578-018-0051-6

Birring, S. S., & Peake, M. D. (2005). Symptoms and the early diagnosis of lung cancer. *Thorax, 60*(4), 268-269. doi:10.1136/thx.2004.032698

Bissell, M. J., Hall, H. G., & Parry, G. (1982). How does the extracellular matrix direct gene expression? *Journal of theoretical biology, 99*(1), 31-68.

Block, J., Breitsprecher, D., Kühn, S., Winterhoff, M., Kage, F., Geffers, R., . . . Brakebusch, C. (2012). FMNL2 drives actin-based protrusion and migration downstream of Cdc42. *Current biology, 22*(11), 1005-1012.

Bradley, S. H., Kennedy, M. P. T., & Neal, R. D. (2019). Recognising Lung Cancer in Primary Care. *Adv Ther, 36*(1), 19-30. doi:10.1007/s12325-018-0843-5

Burgstaller, G., Oehrle, B., Gerckens, M., White, E. S., Schiller, H. B., & Eickelberg, O. (2017). The instructive extracellular matrix of the lung: basic composition and alterations in chronic lung disease. *Eur Respir J, 50*(1). doi:10.1183/13993003.01805-2016

Burridge, K., & Guilluy, C. (2016). Focal adhesions, stress fibers and mechanical tension. *Experimental cell research, 343*(1), 14-20.

Burridge, K., & Wennerberg, K. (2004). Rho and Rac take center stage. *cell, 116*(2), 167-179.

Carter, S. B. (1967). Haptotaxis and the Mechanism of Cell Motility. *Nature, 213*(5073), 256-260. doi:10.1038/213256a0

Chen, M., Jiang, R., Deng, N., Zhao, X., Li, X., & Guo, C. (2022). Natural polymer-based scaffolds for soft tissue repair. *Frontiers in Bioengineering and Biotechnology, 10*, 954699.

Chen, Y., Terajima, M., Yang, Y., Sun, L., Ahn, Y.-H., Pankova, D., . . . Blackmon, S. H. (2015). Lysyl hydroxylase 2 induces a collagen cross-link switch in tumor stroma. *The Journal of clinical investigation, 125*(3), 1147-1162.

Chen, Z., Fillmore, C. M., Hammerman, P. S., Kim, C. F., & Wong, K. K. (2014). Non-small-cell lung cancers: a heterogeneous set of diseases. *Nat Rev Cancer, 14*(8), 535-546. doi:10.1038/nrc3775

Chrzanowska-Wodnicka, M., & Burridge, K. (1996). Rho-stimulated contractility drives the formation of stress fibers and focal adhesions. *J Cell Biol, 133*(6), 1403-1415.

Corrales, L., Rosell, R., Cardona, A. F., Martín, C., Zatarain-Barrón, Z. L., & Arrieta, O. (2020). Lung cancer in never smokers: The role of different risk factors other than tobacco smoking. *Crit Rev Oncol Hematol, 148*, 102895. doi:10.1016/j.critrevonc.2020.102895

Cox, T. R., Bird, D., Baker, A.-M., Barker, H. E., Ho, M. W., Lang, G., & Erler, J. T. (2013). LOX-mediated collagen crosslinking is responsible for fibrosis-enhanced metastasis. *Cancer Res, 73*(6), 1721-1732.
Cox, T. R., & Erler, J. T. (2011). Remodeling and homeostasis of the extracellular matrix: implications for fibrotic diseases and cancer. *Dis Model Mech, 4*(2), 165-178. doi:10.1242/dmm.004077
Csapo, R., Gumpenberger, M., & Wessner, B. (2020). Skeletal muscle extracellular matrix–what do we know about its composition, regulation, and physiological roles? A narrative review. *Frontiers in physiology, 11*, 253.
Dasgupta, I., & McCollum, D. (2019). Control of cellular responses to mechanical cues through YAP/TAZ regulation. *Journal of Biological Chemistry, 294*(46), 17693-17706.
Dillekås, H., Rogers, M. S., & Straume, O. (2019). Are 90% of deaths from cancer caused by metastases? *Cancer medicine, 8*(12), 5574-5576.
Discher, D. E., Janmey, P., & Wang, Y.-l. (2005). Tissue cells feel and respond to the stiffness of their substrate. *Science, 310*(5751), 1139-1143.
Discher, D. E., Janmey, P., & Wang, Y. L. (2005). Tissue cells feel and respond to the stiffness of their substrate. *Science, 310*(5751), 1139-1143. doi:10.1126/science.1116995
Discher, D. E., Mooney, D. J., & Zandstra, P. W. (2009). Growth factors, matrices, and forces combine and control stem cells. *Science, 324*(5935), 1673-1677. doi:10.1126/science.1171643
Dolhnikoff, M., Mauad, T., & Ludwig, M. S. (1999). Extracellular matrix and oscillatory mechanics of rat lung parenchyma in bleomycin-induced fibrosis. *American journal of respiratory and critical care medicine, 160*(5), 1750-1757.
DuChez, B. J., Doyle, A. D., Dimitriadis, E. K., & Yamada, K. M. (2019). Durotaxis by Human Cancer Cells. *Biophys J, 116*(4), 670-683. doi:10.1016/j.bpj.2019.01.009
Emon, B., Bauer, J., Jain, Y., Jung, B., & Saif, T. (2018). Biophysics of tumor microenvironment and cancer metastasis-a mini review. *Computational and structural biotechnology journal, 16*, 279-287.
Engler, A., Bacakova, L., Newman, C., Hategan, A., Griffin, M., & Discher, D. (2004). Substrate compliance versus ligand density in cell on gel responses. *Biophysical journal, 86*(1), 617-628.
Engler, A. J., Richert, L., Wong, J. Y., Picart, C., & Discher, D. E. (2004). Surface probe measurements of the elasticity of sectioned tissue, thin gels and polyelectrolyte multilayer films: correlations between substrate stiffness and cell adhesion. *Surface science, 570*(1-2), 142-154.
Erler, J. T., & Weaver, V. M. (2009). Three-dimensional context regulation of metastasis. *Clinical & experimental metastasis, 26*, 35-49.
Espina, J. A., Marchant, C. L., & Barriga, E. H. (2022). Durotaxis: the mechanical control of directed cell migration. *Febs j, 289*(10), 2736-2754. doi:10.1111/febs.15862
Fang, S., Dai, Y., Mei, Y., Yang, M., Hu, L., Yang, H., . . . Li, J. (2019). Clinical significance and biological role of cancer-derived type I collagen in lung and esophageal cancers. *Thoracic Cancer, 10*(2), 277-288.
García-Fernández, C., Fornaguera, C., & Borrós, S. (2020). Nanomedicine in Non-Small Cell Lung Cancer: From Conventional Treatments to Immunotherapy. *Cancers (Basel), 12*(6), 1609.
Gattazzo, F., Urciuolo, A., & Bonaldo, P. (2014). Extracellular matrix: a dynamic microenvironment for stem cell niche. *Biochim Biophys Acta, 1840*(8), 2506-2519. doi:10.1016/j.bbagen.2014.01.010
Gerstberger, S., Jiang, Q., & Ganesh, K. (2023). Metastasis. *cell, 186*(8), 1564-1579. doi:https://doi.org/10.1016/j.cell.2023.03.003
Girigoswami, K., Saini, D., & Girigoswami, A. (2021). Extracellular Matrix Remodeling and Development of Cancer. *Stem Cell Reviews and Reports, 17*(3), 739-747. doi:10.1007/s12015-020-10070-1
Gu, Y., Ji, Y., Zhao, Y., Liu, Y., Ding, F., Gu, X., & Yang, Y. (2012). The influence of substrate stiffness on the behavior and functions of Schwann cells in culture. *Biomaterials, 33*(28), 6672-6681.
Gupta, M., Doss, B., Lim, C. T., Voituriez, R., & Ladoux, B. (2016). Single cell rigidity sensing: A complex relationship between focal adhesion dynamics and large-scale actin cytoskeleton remodeling. *Cell Adh Migr, 10*(5), 554-567. doi:10.1080/19336918.2016.1173800
Hadden, W., Young, J., Holle, A., McFetridge, M., Kim, D. Y., Wijesinghe, P., . . . Choi, Y. S. (2017). Stem cell migration and mechanotransduction on linear stiffness gradient hydrogels. *Proceedings of the National Academy of Sciences, 114*, 201618239. doi:10.1073/pnas.1618239114

Hakeem, R. M., Subramanian, B. C., Hockenberry, M. A., King, Z. T., Butler, M. T., Legant, W. R., & Bear, J. E. (2023). A Photopolymerized Hydrogel System with Dual Stiffness Gradients Reveals Distinct Actomyosin-Based Mechano-Responses in Fibroblast Durotaxis. *ACS Nano, 17*(1), 197-211. doi:10.1021/acsnano.2c05941

Hanahan, D., & Weinberg, R. A. (2011). Hallmarks of cancer: the next generation. *cell, 144*(5), 646-674.

Harðardottir, H., Jonsson, S., Gunnarsson, O., Hilmarsdottir, B., Asmundsson, J., Gudmundsdottir, I., . . . Gudbjartsson, T. (2022). [Advances in lung cancer diagnosis and treatment - a review]. *Laeknabladid, 108*(1), 17-29. doi:10.17992/lbl.2022.01.671

Hartman, C. D., Isenberg, B. C., Chua, S. G., & Wong, J. Y. (2016). Vascular smooth muscle cell durotaxis depends on extracellular matrix composition. *Proc Natl Acad Sci U S A, 113*(40), 11190-11195. doi:10.1073/pnas.1611324113

Hartman, C. D., Isenberg, B. C., Chua, S. G., & Wong, J. Y. (2016). Vascular smooth muscle cell durotaxis depends on extracellular matrix composition. *Proceedings of the National Academy of Sciences, 113*(40), 11190-11195.

Hebert, J. D., Myers, S. A., Naba, A., Abbruzzese, G., Lamar, J. M., Carr, S. A., & Hynes, R. O. (2020). Proteomic profiling of the ECM of xenograft breast cancer metastases in different organs reveals distinct metastatic niches. *Cancer Res, 80*(7), 1475-1485.

Hoffman, B. D., Grashoff, C., & Schwartz, M. A. (2011). Dynamic molecular processes mediate cellular mechanotransduction. *Nature, 475*(7356), 316-323.

Huang, Y., Su, J., Liu, J., Yi, X., Zhou, F., Zhang, J., . . . Wu, C. (2022). YAP Activation in Promoting Negative Durotaxis and Acral Melanoma Progression. *Cells, 11*(22), 3543.

Humphrey, J. D., Dufresne, E. R., & Schwartz, M. A. (2014). Mechanotransduction and extracellular matrix homeostasis. *Nat Rev Mol Cell Biol, 15*(12), 802-812. doi:10.1038/nrm3896

Humphrey, J. D., Dufresne, E. R., & Schwartz, M. A. (2014). Mechanotransduction and extracellular matrix homeostasis. *Nature reviews Molecular cell biology, 15*(12), 802-812. doi:10.1038/nrm3896

Humphries, J. D., Byron, A., & Humphries, M. J. (2006). Integrin ligands at a glance. *J Cell Sci, 119*(19), 3901-3903.

Hyde, L., & Hyde, C. I. (1974). Clinical manifestations of lung cancer. *Chest, 65*(3), 299-306. doi:10.1378/chest.65.3.299

Hynes, R. O. (2002). Integrins: bidirectional, allosteric signaling machines. *cell, 110*(6), 673-687.

Hynes, R. O. (2002). Integrins: bidirectional, allosteric signaling machines. *cell, 110*(6), 673-687. doi:10.1016/s0092-8674(02)00971-6

Hynes, R. O. (2004). The emergence of integrins: a personal and historical perspective. *Matrix biology: journal of the International Society for Matrix Biology, 23*(6), 333.

Hynes, R. O. (2009). The extracellular matrix: not just pretty fibrils. *Science, 326*(5957), 1216-1219.

Iismaa, S. E., Mearns, B. M., Lorand, L., & Graham, R. M. (2009). Transglutaminases and disease: lessons from genetically engineered mouse models and inherited disorders. *Physiol Rev, 89*(3), 991-1023.

Ishihara, S., & Haga, H. (2022). Matrix Stiffness Contributes to Cancer Progression by Regulating Transcription Factors. *Cancers (Basel), 14*(4). doi:10.3390/cancers14041049

Isomursu, A., Park, K.-Y., Hou, J., Cheng, B., Mathieu, M., Shamsan, G. A., . . . Odde, D. J. (2022). Directed cell migration towards softer environments. *Nature materials, 21*(9), 1081-1090. doi:10.1038/s41563-022-01294-2

Isomursu, A., Park, K. Y., Hou, J., Cheng, B., Mathieu, M., Shamsan, G. A., . . . Odde, D. J. (2022). Directed cell migration towards softer environments. *Nat Mater, 21*(9), 1081-1090. doi:10.1038/s41563-022-01294-2

Itoh, R. E., Kurokawa, K., Ohba, Y., Yoshizaki, H., Mochizuki, N., & Matsuda, M. (2002). Activation of rac and cdc42 video imaged by fluorescent resonance energy transfer-based single-molecule probes in the membrane of living cells. *Molecular and cellular biology, 22*(18), 6582-6591.

Ji, C., & Huang, Y. (2023). Durotaxis and negative durotaxis: where should cells go? *Commun Biol, 6*(1), 1169. doi:10.1038/s42003-023-05554-y

Jiang, Y., Zhang, H., Wang, J., Liu, Y., Luo, T., & Hua, H. (2022). Targeting extracellular matrix stiffness and mechanotransducers to improve cancer therapy. *Journal of Hematology & Oncology, 15*(1), 34. doi:10.1186/s13045-022-01252-0

Joshi, R. S., Kanugula, S. S., Sudhir, S., Pereira, M. P., Jain, S., & Aghi, M. K. (2021). The Role of Cancer-Associated Fibroblasts in Tumor Progression. *Cancers (Basel), 13*(6). doi:10.3390/cancers13061399

Kalli, M., & Stylianopoulos, T. (2018). Defining the role of solid stress and matrix stiffness in cancer cell proliferation and metastasis. *Frontiers in oncology, 8*, 55.

Kang, C., Chen, P., Yi, X., Li, D., Hu, Y., Yang, Y., . . . Wu, C. (2024). Amoeboid cells undergo durotaxis with soft end polarized NMIIA. *bioRxiv*, 2023.2004.2013.536664. doi:10.1101/2023.04.13.536664

Kaukonen, R., Mai, A., Georgiadou, M., Saari, M., De Franceschi, N., Betz, T., . . . Ivaska, J. (2016). Normal stroma suppresses cancer cell proliferation via mechanosensitive regulation of JMJD1a-mediated transcription. *Nat Commun, 7*, 12237. doi:10.1038/ncomms12237

Kechagia, J. Z., Ivaska, J., & Roca-Cusachs, P. (2019). Integrins as biomechanical sensors of the microenvironment. *Nature reviews Molecular cell biology, 20*(8), 457-473.

Khatiwala, C. B., Peyton, S. R., & Putnam, A. J. (2006). Intrinsic mechanical properties of the extracellular matrix affect the behavior of pre-osteoblastic MC3T3-E1 cells. *Am J Physiol Cell Physiol, 290*(6), C1640-1650. doi:10.1152/ajpcell.00455.2005

Koser, D. E., Thompson, A. J., Foster, S. K., Dwivedy, A., Pillai, E. K., Sheridan, G. K., . . . Franze, K. (2016). Mechanosensing is critical for axon growth in the developing brain. *Nat Neurosci, 19*(12), 1592-1598. doi:10.1038/nn.4394

Kretschmer, R. R., & Collado, M. L. (1980). Chemotaxis. *Infection, 8 Suppl 3*, S 299-302. doi:10.1007/bf01639599

Kular, J. K., Basu, S., & Sharma, R. I. (2014). The extracellular matrix: Structure, composition, age-related differences, tools for analysis and applications for tissue engineering. *J Tissue Eng, 5*, 2041731414557112. doi:10.1177/2041731414557112

Lachowski, D., Cortes, E., Pink, D., Chronopoulos, A., Karim, S. A., J, P. M., & Del Río Hernández, A. E. (2017). Substrate Rigidity Controls Activation and Durotaxis in Pancreatic Stellate Cells. *Sci Rep, 7*(1), 2506. doi:10.1038/s41598-017-02689-x

Lachowski, D., Cortes, E., Robinson, B., Rice, A., Rombouts, K., & Del Río Hernández, A. E. (2018). FAK controls the mechanical activation of YAP, a transcriptional regulator required for durotaxis. *Faseb j, 32*(2), 1099-1107. doi:10.1096/fj.201700721R

Ladoux, B., Mège, R.-M., & Trepat, X. (2016). Front–rear polarization by mechanical cues: from single cells to tissues. *Trends in cell biology, 26*(6), 420-433.

Lee, D., Golden, K., Rahman, M. M., Moran, A., Gonzalez, B., & Ryu, S. (2019). Fabrication of Hydrogels with a Stiffness Gradient Using Limited Mixing in the Hele-Shaw Geometry. *Experimental Mechanics, 59*(9), 1249-1259. doi:10.1007/s11340-018-0416-1

Lee, J., Condello, S., Yakubov, B., Emerson, R., Caperell-Grant, A., Hitomi, K., . . . Matei, D. (2015). Tissue transglutaminase mediated tumor–stroma interaction promotes pancreatic cancer progression. *Clinical Cancer Research, 21*(19), 4482-4493.

Liu, Z., & Vunjak-Novakovic, G. (2016). Modeling tumor microenvironments using custom-designed biomaterial scaffolds. *Curr Opin Chem Eng, 11*, 94-105. doi:10.1016/j.coche.2016.01.012

Lo, C.-M., Wang, H.-B., Dembo, M., & Wang, Y.-l. (2000). Cell Movement Is Guided by the Rigidity of the Substrate. *Biophysical journal, 79*(1), 144-152. doi:https://doi.org/10.1016/S0006-3495(00)76279-5

Mak, I. W., Evaniew, N., & Ghert, M. (2014). Lost in translation: animal models and clinical trials in cancer treatment. *American journal of translational research, 6*(2), 114.

McKee, T. J., Perlman, G., Morris, M., & Komarova, S. V. (2019). Extracellular matrix composition of connective tissues: a systematic review and meta-analysis. *Scientific reports, 9*(1), 10542.

Meyerson, M., Franklin, W. A., & Kelley, M. J. (2004). Molecular classification and molecular genetics of human lung cancers. *Semin Oncol, 31*(1 Suppl 1), 4-19. doi:10.1053/j.seminoncol.2003.12.009

Miyazawa, A., Ito, S., Asano, S., Tanaka, I., Sato, M., Kondo, M., & Hasegawa, Y. (2018). Regulation of PD-L1 expression by matrix stiffness in lung cancer cells. *Biochemical and biophysical research communications, 495*(3), 2344-2349.

MOORE, B. R. (1980). A modification of the Rayleigh test for vector data. *Biometrika, 67*(1), 175-180. doi:10.1093/biomet/67.1.175

Moore, K. A., Polte, T., Huang, S., Shi, B., Alsberg, E., Sunday, M. E., & Ingber, D. E. (2005). Control of basement membrane remodeling and epithelial branching morphogenesis in embryonic lung by Rho and cytoskeletal tension. *Developmental dynamics: an official publication of the American Association of Anatomists, 232*(2), 268-281.

Moore, S. W., Roca-Cusachs, P., & Sheetz, M. P. (2010). Stretchy proteins on stretchy substrates: the important elements of integrin-mediated rigidity sensing. *Developmental cell, 19*(2), 194-206.

Mycielska, M. E., & Djamgoz, M. B. (2004). Cellular mechanisms of direct-current electric field effects: galvanotaxis and metastatic disease. *J Cell Sci, 117*(Pt 9), 1631-1639. doi:10.1242/jcs.01125

Naba, A., Clauser, K. R., Hoersch, S., Liu, H., Carr, S. A., & Hynes, R. O. (2012). The matrisome: in silico definition and in vivo characterization by proteomics of normal and tumor extracellular matrices. *Mol Cell Proteomics, 11*(4), M111.014647. doi:10.1074/mcp.M111.014647

Naba, A., Clauser, K. R., Hoersch, S., Liu, H., Carr, S. A., & Hynes, R. O. (2012). The matrisome: in silico definition and in vivo characterization by proteomics of normal and tumor extracellular matrices. *Molecular & Cellular Proteomics, 11*(4).

Navab, R., Strumpf, D., To, C., Pasko, E., Kim, K. S., Park, C. J., . . . Tsao, M. S. (2016). Integrin α11β1 regulates cancer stromal stiffness and promotes tumorigenicity and metastasis in non-small cell lung cancer. *Oncogene, 35*(15), 1899-1908. doi:10.1038/onc.2015.254

Nicholson, A. G., Tsao, M. S., Beasley, M. B., Borczuk, A. C., Brambilla, E., Cooper, W. A., . . . Travis, W. D. (2022). The 2021 WHO Classification of Lung Tumors: Impact of Advances Since 2015. *J Thorac Oncol, 17*(3), 362-387. doi:10.1016/j.jtho.2021.11.003

Nishimura, T., & Kaibuchi, K. (2007). Numb controls integrin endocytosis for directional cell migration with aPKC and PAR-3. *Developmental cell, 13*(1), 15-28.

Nukuda, A., Sasaki, C., Ishihara, S., Mizutani, T., Nakamura, K., Ayabe, T., . . . Haga, H. (2015). Stiff substrates increase YAP-signaling-mediated matrix metalloproteinase-7 expression. *Oncogenesis, 4*(9), e165-e165.

Oakes, P. W., Bidone, T. C., Beckham, Y., Skeeters, A. V., Ramirez-San Juan, G. R., Winter, S. P., . . . Gardel, M. L. (2018). Lamellipodium is a myosin-independent mechanosensor. *Proceedings of the National Academy of Sciences, 115*(11), 2646-2651.

Pandya, P., Orgaz, J. L., & Sanz-Moreno, V. (2017). Actomyosin contractility and collective migration: may the force be with you. *Curr Opin Cell Biol, 48*, 87-96.

Pandya, P., Orgaz, J. L., & Sanz-Moreno, V. (2017). Modes of invasion during tumour dissemination. *Molecular oncology, 11*(1), 5-27.

Pankova, D., Chen, Y., Terajima, M., Schliekelman, M. J., Baird, B. N., Fahrenholtz, M., . . . Kurie, J. M. (2016). Cancer-Associated Fibroblasts Induce a Collagen Cross-link Switch in Tumor Stroma. *Mol Cancer Res, 14*(3), 287-295. doi:10.1158/1541-7786.mcr-15-0307

Parisi, L., Toffoli, A., Ghezzi, B., Mozzoni, B., Lumetti, S., & Macaluso, G. M. (2020). A glance on the role of fibronectin in controlling cell response at biomaterial interface. *Japanese dental science review, 56*(1), 50-55.

Park, J., Kim, D.-H., & Levchenko, A. (2018). Topotaxis: A New Mechanism of Directed Cell Migration in Topographic ECM Gradients. *Biophysical journal, 114*(6), 1257-1263. doi:https://doi.org/10.1016/j.bpj.2017.11.3813

Pelham Jr, R. J., & Wang, Y.-l. (1997). Cell locomotion and focal adhesions are regulated by substrate flexibility. *Proceedings of the National Academy of Sciences, 94*(25), 13661-13665.

Peyton, S. R., & Putnam, A. J. (2005). Extracellular matrix rigidity governs smooth muscle cell motility in a biphasic fashion. *Journal of cellular physiology, 204*(1), 198-209.

Plikus, M. V., Wang, X., Sinha, S., Forte, E., Thompson, S. M., Herzog, E. L., . . . Horsley, V. (2021). Fibroblasts: Origins, definitions, and functions in health and disease. *cell, 184*(15), 3852-3872.

Plotnikov, S. V., Pasapera, A. M., Sabass, B., & Waterman, C. M. (2012). Force fluctuations within focal adhesions mediate ECM-rigidity sensing to guide directed cell migration. *cell, 151*(7), 1513-1527. doi:10.1016/j.cell.2012.11.034

Pradhan, S., Clary, J. M., Seliktar, D., & Lipke, E. A. (2017). A three-dimensional spheroidal cancer model based on PEG-fibrinogen hydrogel microspheres. *Biomaterials, 115*, 141-154.

Raab, M., Swift, J., P. Dingal, P. D., Shah, P., Shin, J.-W., & Discher, D. E. (2012). Crawling from soft to stiff matrix polarizes the cytoskeleton and phosphoregulates myosin-II heavy chain. *Journal of Cell Biology, 199*(4), 669-683.

Reid, S. E., Kay, E. J., Neilson, L. J., Henze, A. T., Serneels, J., McGhee, E. J., . . . Santi, A. (2017). Tumor matrix stiffness promotes metastatic cancer cell interaction with the endothelium. *Embo j, 36*(16), 2373-2389.

Rong, Y., Yang, W., Hao, H., Wang, W., Lin, S., Shi, P., . . . Wu, C. (2021). The Golgi microtubules regulate single cell durotaxis. *EMBO Rep, 22*(3), e51094. doi:10.15252/embr.202051094

Schindelin, J., Arganda-Carreras, I., Frise, E., Kaynig, V., Longair, M., Pietzsch, T., . . . Cardona, A. (2012). Fiji: an open-source platform for biological-image analysis. *Nat Methods, 9*(7), 676-682. doi:10.1038/nmeth.2019

Schrader, J., Gordon-Walker, T. T., Aucott, R. L., van Deemter, M., Quaas, A., Walsh, S., . . . Iredale, J. P. (2011). Matrix stiffness modulates proliferation, chemotherapeutic response, and dormancy in hepatocellular carcinoma cells. *Hepatology, 53*(4), 1192-1205.

Schwartz, M. A. (2010). Integrins and extracellular matrix in mechanotransduction. *Cold Spring Harbor perspectives in biology, 2*(12), a005066.

Senior, R. M., Bielefeld, D. R., & Abensohn, M. K. (1975). The effects of proteolytic enzymes on the tensile strength of human lung. *American Review of Respiratory Disease, 111*(2), 184-188.

Shellard, A., & Mayor, R. (2021a). Collective durotaxis along a self-generated stiffness gradient in vivo. *Nature, 600*(7890), 690-694.

Shellard, A., & Mayor, R. (2021b). Durotaxis: the hard path from in vitro to in vivo. *Developmental cell, 56*(2), 227-239.

Shi, J., Hua, X., Zhu, B., Ravichandran, S., Wang, M., Nguyen, C., . . . Landi, M. T. (2016). Somatic Genomics and Clinical Features of Lung Adenocarcinoma: A Retrospective Study. *PLoS Med, 13*(12), e1002162. doi:10.1371/journal.pmed.1002162

Siddiqui, F., Vaqar, S., & Siddiqui, A. H. (2023). Lung Cancer *StatPearls*. Treasure Island (FL) ineligible companies. Disclosure: Sarosh Vaqar declares no relevant financial relationships with ineligible companies. Disclosure: Abdul Siddiqui declares no relevant financial relationships with ineligible companies.: StatPearls Publishing

Copyright © 2023, StatPearls Publishing LLC.

Siegel, R. L., Miller, K. D., Fuchs, H. E., & Jemal, A. (2022). Cancer statistics, 2022. *CA Cancer J Clin, 72*(1), 7-33. doi:10.3322/caac.21708

Siegel, R. L., Miller, K. D., & Jemal, A. (2020). Cancer statistics, 2020. *CA Cancer J Clin, 70*(1), 7-30. doi:10.3322/caac.21590

Singh, S. P., Schwartz, M. P., Lee, J. Y., Fairbanks, B. D., & Anseth, K. S. (2014). A peptide functionalized poly (ethylene glycol)(PEG) hydrogel for investigating the influence of biochemical and biophysical matrix properties on tumor cell migration. *Biomaterials science, 2*(7), 1024-1034.

Socovich, A. M., & Naba, A. (2019). *The cancer matrisome: From comprehensive characterization to biomarker discovery.* Paper presented at the Seminars in cell & developmental biology.

Suki, B., Ito, S., Stamenovic, D., Lutchen, K. R., & Ingenito, E. P. (2005). Biomechanics of the lung parenchyma: critical roles of collagen and mechanical forces. *Journal of applied physiology, 98*(5), 1892-1899.

Sunyer, R., Jin, A. J., Nossal, R., & Sackett, D. L. (2012). Fabrication of hydrogels with steep stiffness gradients for studying cell mechanical response. *PLoS One, 7*(10), e46107. doi:10.1371/journal.pone.0046107

Sunyer, R., & Trepat, X. (2020). Durotaxis. *Current biology, 30*(9), R383-R387.
Takada, Y., Ye, X., & Simon, S. (2007). The integrins. *Genome Biol, 8*(5), 215. doi:10.1186/gb-2007-8-5-215
Tanaka, R., & Ludwig, M. (1999). Changes in viscoelastic properties of rat lung parenchymal strips with maturation. *Journal of applied physiology, 87*(6), 2081-2089.
Tang, R. Z., & Liu, X. Q. (2023). Biophysical cues of in vitro biomaterials-based artificial extracellular matrix guide cancer cell plasticity. *Mater Today Bio, 19*, 100607. doi:10.1016/j.mtbio.2023.100607
Travis, W., Brambilla, E., Muller-Hermelink, H., & Harris, C. World Health Organization Classification of Tumours: Pathology and Genetics of Tumours of the Lung, Pleura, Thymus and Heart 2004 Lyon: France IARC Press.
Tse, J. R., & Engler, A. J. (2010). Preparation of hydrogel substrates with tunable mechanical properties. *Curr Protoc Cell Biol, Chapter 10*, Unit 10.16. doi:10.1002/0471143030.cb1016s47
Tsutsui, K., Machida, H., Nakagawa, A., Ahn, K., Morita, R., Sekiguchi, K., . . . Fujiwara, H. (2021). Mapping the molecular and structural specialization of the skin basement membrane for inter-tissue interactions. *Nature communications, 12*(1), 2577. doi:10.1038/s41467-021-22881-y
Tweedy, L., Knecht, D. A., Mackay, G. M., & Insall, R. H. (2016). Self-Generated Chemoattractant Gradients: Attractant Depletion Extends the Range and Robustness of Chemotaxis. *PLoS Biol, 14*(3), e1002404. doi:10.1371/journal.pbio.1002404
Umesh, V., Rape, A. D., Ulrich, T. A., & Kumar, S. (2014). Microenvironmental stiffness enhances glioma cell proliferation by stimulating epidermal growth factor receptor signaling. *PLoS One, 9*(7), e101771.
Vincent, L. G., Choi, Y. S., Alonso-Latorre, B., Del Álamo, J. C., & Engler, A. J. (2013). Mesenchymal stem cell durotaxis depends on substrate stiffness gradient strength. *Biotechnology journal, 8*(4), 472-484.
Vining, K. H., & Mooney, D. J. (2017). Mechanical forces direct stem cell behaviour in development and regeneration. *Nat Rev Mol Cell Biol, 18*(12), 728-742. doi:10.1038/nrm.2017.108
Walma, D. A. C., & Yamada, K. M. (2020). The extracellular matrix in development. *Development, 147*(10). doi:10.1242/dev.175596
Wang, X., Ji, L., Wang, J., & Liu, C. (2023). Matrix stiffness regulates osteoclast fate through integrin-dependent mechanotransduction. *Bioact Mater, 27*, 138-153. doi:10.1016/j.bioactmat.2023.03.014
Wei, S. C., & Yang, J. (2016). Forcing through tumor metastasis: the interplay between tissue rigidity and epithelial–mesenchymal transition. *Trends in cell biology, 26*(2), 111-120.
Winkler, J., Abisoye-Ogunniyan, A., Metcalf, K. J., & Werb, Z. (2020). Concepts of extracellular matrix remodelling in tumour progression and metastasis. *Nature communications, 11*(1), 5120.
Wisdom, K. M., Adebowale, K., Chang, J., Lee, J. Y., Nam, S., Desai, R., . . . Hodgson, L. (2018). Matrix mechanical plasticity regulates cancer cell migration through confining microenvironments. *Nature communications, 9*(1), 4144.
Wong, S., Guo, W.-H., & Wang, Y.-L. (2014). Fibroblasts probe substrate rigidity with filopodia extensions before occupying an area. *Proceedings of the National Academy of Sciences, 111*(48), 17176-17181.
Worthylake, R. A., & Burridge, K. (2003). RhoA and ROCK promote migration by limiting membrane protrusions. *Journal of Biological Chemistry, 278*(15), 13578-13584.
Wrighton, K. H. (2013). The 'ins' and 'outs' of integrin signalling. *Nature reviews Molecular cell biology, 14*(12), 753-753. doi:10.1038/nrm3708
Xin, S., Dai, J., Gregory, C. A., Han, A., & Alge, D. L. (2020). Creating physicochemical gradients in modular microporous annealed particle hydrogels via a microfluidic method. *Advanced functional materials, 30*(6), 1907102.
Yamada, K. M., & Sixt, M. (2019). Mechanisms of 3D cell migration. *Nature reviews Molecular cell biology, 20*(12), 738-752.
Yeoman, B., Shatkin, G., Beri, P., Banisadr, A., Katira, P., & Engler, A. J. (2021). Adhesion strength and contractility enable metastatic cells to become adurotactic. *Cell Rep, 34*(10), 108816. doi:10.1016/j.celrep.2021.108816
Yi, B., Xu, Q., & Liu, W. (2022). An overview of substrate stiffness guided cellular response and its applications in tissue regeneration. *Bioact Mater, 15*, 82-102. doi:10.1016/j.bioactmat.2021.12.005

Yuan, Y., Zhong, W., Ma, G., Zhang, B., & Tian, H. (2015). Yes-associated protein regulates the growth of human non-small cell lung cancer in response to matrix stiffness. *Molecular medicine reports, 11*(6), 4267-4272.

Zaidel-Bar, R., Itzkovitz, S., Ma'ayan, A., Iyengar, R., & Geiger, B. (2007). Functional atlas of the integrin adhesome. *Nature cell biology, 9*(8), 858-867.

Zeltz, C., & Gullberg, D. (2016). The integrin–collagen connection–a glue for tissue repair? *J Cell Sci, 129*(4), 653-664.